MRI-Based Quantitative Osteoporosis Imaging at the Spine and Femur

Nico Sollmann MD, PhD,[1,2*] Maximilian T. Löffler MD, MSc,[1] Sophia Kronthaler MSc,[3] Christof Böhm MSc,[3] Michael Dieckmeyer MD,[1] Stefan Ruschke PhD,[3] Jan S. Kirschke MD,[1,2] Julio Carballido-Gamio PhD,[4] Dimitrios C. Karampinos PhD,[3] Roland Krug PhD,[5] and Thomas Baum MD[1]

Osteoporosis is a systemic skeletal disease with a high prevalence worldwide, characterized by low bone mass and microarchitectural deterioration, predisposing an individual to fragility fractures. Dual-energy X-ray absorptiometry (DXA) has been the clinical reference standard for diagnosing osteoporosis and for assessing fracture risk for decades. However, other imaging modalities are of increasing importance to investigate the etiology, treatment, and fracture risk. The purpose of this work is to review the available literature on quantitative magnetic resonance imaging (MRI) methods and related findings in osteoporosis at the spine and proximal femur as the clinically most important fracture sites. Trabecular bone microstructure analysis at the proximal femur based on high-resolution MRI allows for a better prediction of osteoporotic fracture risk than DXA-based bone mineral density (BMD) alone. In the 1990s, T_2* mapping was shown to correlate with the density and orientation of the trabecular bone. Recently, quantitative susceptibility mapping (QSM), which overcomes some of the limitations of T_2* mapping, has been applied for trabecular bone quantifications at the spine, whereas ultrashort echo time (UTE) imaging provides valuable surrogate markers of cortical bone quantity and quality. Magnetic resonance spectroscopy (MRS) and chemical shift encoding-based water–fat MRI (CSE-MRI) enable the quantitative assessment of the nonmineralized bone compartment through extraction of the bone marrow fat fraction (BMFF). Furthermore, CSE-MRI allows for the differentiation of osteoporotic vs. pathologic fractures, which is of high clinical relevance. Lastly, advanced postprocessing and image analysis tools, particularly considering statistical parametric mapping and region-specific BMFF distributions, have high potential to further improve MRI-based fracture risk assessments at the spine and hip.
Level of Evidence: 5
Technical Efficacy Stage: 2

J. MAGN. RESON. IMAGING 2020.

OSTEOPOROSIS is a systemic skeletal disease, characterized by low bone mass and microarchitectural deterioration of bone tissue, predisposing a person to fragility fractures.[1–3] The prevalence of osteoporosis is high, with an estimation of 200 million people currently suffering from the disease worldwide.[4] Further increases in the prevalence are expected, which is due to an aging population and a demographic change.[4,5] Females are generally at higher risk to develop osteoporosis, particularly after the menopause, with about 30% of all postmenopausal women being affected by

View this article online at wileyonlinelibrary.com. DOI: 10.1002/jmri.27260

Received Mar 29, 2020, Accepted for publication Jun 1, 2020.

*Address reprint requests to: N.S., Department of Diagnostic and Interventional Neuroradiology, Klinikum rechts der Isar, Technische Universität München, Ismaninger Str. 22, 81675 Munich, Germany. E-mail: nico.sollmann@tum.de

Contract grant sponsor: European Research Council (ERC); Contract grant number: 677661—ProFatMRI (to D.C.K.); Contract grant number: 637164—iBack (to J.S.K.); Contract grant sponsor: German Research Foundation (Deutsche Forschungsgemeinschaft, DFG); Contract grant number: 432290010 (to J.S.K. & T.B.); Contract grant sponsor: German Society of Musculoskeletal Radiology (Deutsche Gesellschaft für Muskuloskelettale Radiologie, DGMSR) (to N.S. & M.D.). D.C.K. receives grant support from Philips Healthcare. The authors acknowledge funding from the TUM Institute for Advanced Study for a TUM August-Wilhelm Scheer Visiting Professorship of Dr. Krug.

From the [1]Department of Diagnostic and Interventional Neuroradiology, Klinikum rechts der Isar, Technische Universität München, Munich, Germany; [2]TUM-Neuroimaging Center, Klinikum rechts der Isar, Technische Universität München, Munich, Germany; [3]Department of Diagnostic and Interventional Radiology, Klinikum rechts der Isar, Technische Universität München, Munich, Germany; [4]Department of Radiology, School of Medicine, University of Colorado Anschutz Medical Campus, Aurora, Colorado, USA; and [5]Department of Radiology and Biomedical Imaging, School of Medicine, University of California San Francisco, San Francisco, California, USA

osteoporosis in Western countries, resulting in one or more fragility fractures among ~40% of these women in their remaining lifetime.[6,7] Among the male counterparts, still about 15% to 30% are expected to sustain at least one fragility fracture during life, making osteoporosis a public health concern.[7] Osteoporotic fragility fractures have been shown to considerably reduce health-related quality of life and to lead to premature mortality.[8–12] In this context, the presence of the initial fracture has been identified as a main risk factor for later additional fractures, with an increased risk of about 86% for a new fracture among people who have already sustained a fracture.[13]

Vertebral fractures are estimated to be the most frequently occurring fractures in osteoporosis.[1–3] Affected subjects present a 2.3-fold increase in the risk of future hip fracture, a 1.6-fold increase in the risk of future distal forearm fracture, and a considerable 12.6-fold increase in the risk of future additional vertebral fractures.[14] Despite their frequent occurrence, osteoporotic vertebral fractures often remain hidden and can stay asymptomatic, with fewer than 10% of such fractures resulting in hospitalization, even in cases with symptoms.[15,16] Consequently, initiation of treatment can become drastically delayed, which is particularly problematic in the light of the increased risk for future additional fractures.[14]

Following vertebral fractures, hip fractures represent the second most frequent osteoporotic fractures.[1–3] In contrast to osteoporotic vertebral fractures, hip fractures rarely stay silent, leading to high hospitalization rates including surgical treatment among affected people. Particularly after hip fractures, an increased risk of death can be observed in osteoporotic subjects, which is highest in the days and weeks following the fracture, remains elevated for months, and is causally related to 20–30% of deaths.[17–19] Moreover, only 40–60% of hip fracture patients can recover to their prefracture status of mobility, with 20–60% of patients who were independent in self-care activities before the fracture requiring assistance to perform these tasks after one year.[20,21]

The management of osteoporosis largely aims at preventing fractures and/or at therapy of related complications.[1–3] In this regard, the objective of osteoporosis treatment is to lower the likelihood of fragility fractures by strengthening the skeleton, decreasing fall frequency, or both.[2] Besides recommendations of adaption of lifestyle factors (eg, regular physical activity and good nutrition), pharmacological interventions are appropriate for osteoporosis treatment, particularly in subjects with a high risk profile.[2] Several drugs have been shown to substantially decrease fracture risk by ~30–70% for vertebral fractures and by as much as ~50% for hip fractures.[2] Bisphosphonates are the most commonly used drugs in osteoporosis and, as antiresorptive agents, are capable of inhibiting osteoclasts to avoid or slow down further bone weakening, thus reducing fracture risks.[22,23] While bisphosphonates only have moderate effects on bone mineral density (BMD), newer drug options, such as denosumab or teriparatide, can facilitate a progressive BMD increase and provide the possibility that a specific BMD value may be defined to guide osteoporosis treatment decisions.[2,24] Furthermore, in subjects who have already sustained an osteoporotic fracture, surgery may be considered as a treatment option. While almost all hip fractures require timely surgery, conservative treatment could generally be appropriate for a considerable proportion of vertebral fractures except for cases with complications such as fracture-associated neurological deficits, high pain intensity and lasting immobility, significant instability, and/or progressing fracture sintering.[25–27]

Areal BMD derived from dual-energy X-ray absorptiometry (DXA) of the spine and/or hip is the clinical standard for diagnosing osteoporosis and for assessing fracture risk.[1,28,29] However, it is well known that DXA has important limitations that can interfere with correct detection of osteoporosis, and that the DXA-based T-score—the diagnostic value for osteoporosis—is not appropriate as the sole factor to identify patients at high fracture risk. Specifically, it has been shown that DXA-derived BMD values of subjects with and without osteoporosis can overlap.[30,31] Thus, other techniques, including quantitative computed tomography (QCT) and magnetic resonance imaging (MRI), over the last years have experienced increasing attention for imaging-based studies of etiology, fracture risk assessment, and therapy monitoring. Recent reviews have highlighted the current and potential future role of QCT for osteoporosis diagnosis and monitoring.[32–34]

Regarding quantitative MRI, studies dating back to the 1990s introduced T_2* mapping and high-resolution trabecular bone imaging, which can enable the assessment of bone microstructure that is relevant in the context of osteoporosis.[35–37] In the 2000s, MRI studies started to demonstrate that bone marrow (BM), which fills the cavities of trabecular bone and mainly consists of adipocytes (yellow marrow regions) and hematopoietic red blood cells (red marrow regions), may play a key role in bone health and metabolism, with distinct alterations becoming increasingly evident in osteoporotic subjects.[38,39] MRI techniques to investigate the BM fat fraction (BMFF) include magnetic resonance spectroscopy (MRS) and chemical shift encoding-based water-fat MRI (CSE-MRI). However, a variety of other MRI methods, such as ultrashort echo time (UTE) imaging of cortical bone and quantitative susceptibility mapping (QSM) for imaging of trabecular bone, have recently found their way into the repertoire of MRI techniques for osteoporosis assessment.[40–42] While early MRI methods predominantly exploited the signal arising from BM to image the trabecular microstructure of bone, more recent approaches like UTE imaging and QSM enable more direct imaging of bone tissue and have only recently been applied to imaging of the spine.

The purpose of this article is to review the current literature on quantitative MRI methods and related findings in osteoporosis at the spine and proximal femur from a methodological and clinical perspective.

Assessment of Trabecular Bone Microstructure

Background

The MRI signal from solid-state tissues such as bone is very low because of short T_2* and, thus, trabecular bone appears dark in most clinical sequences. Hence, the ability to image the trabecular network is due to strong signal from the fatty BM, which surrounds the trabecular bone structure. Consequently, the goal of MRI acquisition is to maximize the BM signal and enhance the contrast to the cancellous bone.[36,43] Table 1 gives an overview of the technique's main characteristics in relation to other sequences.

Technical Principles

In general, approaches to assess trabecular bone microarchitecture in vivo have been reported for MRI at 1.5T and 3T. High-resolution imaging to depict the trabecular bone microarchitecture of the proximal femur has been challenging, and at the spine is currently not feasible due to signal-to-noise ratio (SNR) constraints. The proximal femur is relatively deep in the human body and, hence, the signal response decays quickly. Furthermore, the proximal femur contains higher amounts of hematopoietic BM compared to the fattier BM in the extremities such as in the wrist or ankle. Hematopoietic BM has longer T_1 recovery times and therefore is usually darker in MRI. However, with the advent of higher field strengths, and advanced RF coils, the first in vivo high-resolution MRI of the proximal femur enabling trabecular bone analysis was published about 15 years ago.[44] Images featured a spatial resolution of 234 μm in-plane and 1500 μm slice thickness.[44] Since then, further progress has been made towards higher spatial resolution and better image quality. Current state-of-the-art in vivo MRI acquisition at the proximal femur can achieve a spatial resolution of 234 μm in-plane and 500 μm slice thickness in a clinically feasible scan time.[43, 45]

Initially, mainly gradient-echo-based pulse sequences were used for high-resolution imaging of the proximal femur.[43–48] The advantage of this type of pulse sequence is the high SNR efficiency and, thus, a shorter scan time. Some disadvantages include the susceptibility-induced broadening of the trabecular bone structure.[49] Furthermore, the prevalence of hematopoietic BM in some areas of the proximal femur limits the signal in these regions. For these reasons, a spin-echo-based pulse sequence (OVS-CUBE) has been proposed for trabecular bone MRI of the proximal femur.[50] OVS-CUBE combines a multi-spin-echo variable flip angle approach with outer volume suppression. The spin-echo implementation limits susceptibility-induced effects and optimizes signal from the hematopoietic BM by allowing longer repetition times (TRs) (Fig. 1).

Image postprocessing plays an essential role for assessment of trabecular bone microstructure. The first step of postprocessing includes correction of the coil intensity inhomogeneity. A simple method is based on low-pass filtering, whereas more advanced coil correction approaches include a fully-automated scheme based on a nonparametric, non-uniform intensity normalization approach that preserves image information while accurately correcting for coil-induced intensity inhomogeneities.[51–53] After correcting for the coil inhomogeneity and segmentation, the trabecular bone's microstructural information can be extracted. This commonly includes bone volume fraction (BVF) or bone volume to total volume fraction, trabecular thickness, trabecular spacing, and trabecular number.[54] All these parameters are usually titled "apparent" as they correlate well with true values from micro-CT, but absolute values may differ.[55] For analysis of the proximal femur, mainly fuzzy clustering with local bone enhancement at multiple scales has been used to obtain the BVF.[56,57] All other parameters are then obtained by thresholding the BVF map.[54] However, several other methods exist, including digital topological analysis, geodesic topological analysis, local inertial anisotropy, volumetric topological analysis, and tensor scale analysis.[58–64] Finite element analysis (FEA) has also been previously used to compute the elastic modulus and to measure bone strength.[65–67] In this regard, FEA applied to MRI data has shown to be a promising approach that can reliably provide fracture risk information and evaluation of bone strength with good reproducibility of FEA measurements, furthermore pointing at good agreement of the method against the gold standard of mechanical testing at the femur.[47,68–70]

Application and Main Findings

In vivo microstructural analysis of high-resolution MRI of the proximal femur has been clinically applied to postmenopausal women with osteoporosis,[47,71] long-term glucocorticoid users,[48] as well as human immunodeficiency virus-infected (HIV) men.[45] Patients with fractures had lower elastic modulus than the control group in all proximal femur regions but no differences in T-scores.[47] Another study investigated 60 postmenopausal women (30 with and 30 without fragility fractures) who did not have osteoporotic BMD in the proximal femur; however, the fracture group was found to have significantly impaired bone microstructure.[71] One study in eight HIV-infected men found significantly lower bone quality compared to healthy controls, but BMD did not show significant differences between HIV-infected patients and healthy controls.[45] These findings suggest that assessment of trabecular bone microarchitecture might play an important

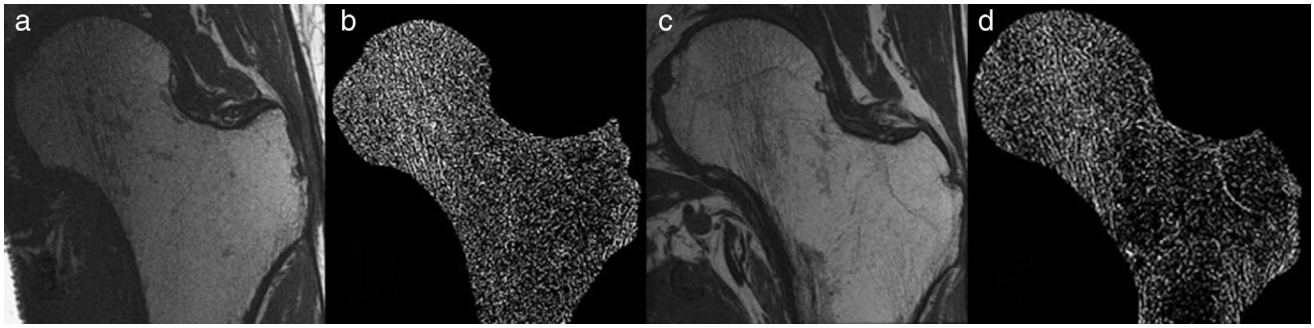

FIGURE 1: Spin-echo-based pulse sequence (OVS-CUBE) at the proximal femur. High-resolution images of the proximal femur acquired with an OVS-CUBE sequence: (a) the hip of a healthy male control, (b) trabecular structure after fuzzy thresholding of the control scan, (c) image of an age-matched male subject with human immunodeficiency virus (HIV) infection, and (d) trabecular structure of the scan of the subject infected with HIV. It can be seen that the trabecular structure is less dense in the HIV-infected subject, in particular in the neck, trochanter, and shaft of the femur. The images were first N3-coil corrected, fuzzy clustered, and thresholded. Sequence details (OVS-CUBE): A train of 10 echoes with variable flip angles were acquired with an echo spacing of 8.3 msec and TR = 500 msec. The spatial resolution achieved was 234 × 234 × 700 μm^3.

role in the context of bone quality in addition to BMD measurements.

T_2* and Quantitative Susceptibility Mapping

Background

T_2* mapping was the first quantitative MRI technique for assessment of bone as reported in the 1990s.[35–37] Bone is more diamagnetic than marrow. In the trabecular bone and BM interface, the two coexisting phases induce local magnetic field inhomogeneities. This can be measured as a shortening of the effective transverse relaxation time. It has been demonstrated that T_2* correlates with the density and orientation of the trabecular bone.[36] A more direct measurement of the susceptibility difference between the vertebral trabecularized BM and surrounding tissues is based on QSM (Table 1).

Technical Principles

The method of QSM can overcome the limitation of T_2* relaxometry that para- and diamagnetic susceptibility sources similarly result in an increased relaxation rate (Fig. 2). In general, QSM has been proven to be capable of providing quantitative and reproducible data on magnetic susceptibility of different tissues of the body.[72] However, due to the fact that bone has a considerably shorter transverse relaxation time in combination with low signal at commonly used echo times (TEs) in gradient echo imaging, evaluation of osseous structures remains challenging.[42,72] It has been suggested that QSM of BM can be biased due to the low signal of cortical bone structures in the proximity of trabecularized BM.[42,73] Consequently, UTE might be important to correctly estimate susceptibility of musculoskeletal anatomies and, thus, could be relevant for derived BMD values in trabecularized BM. However, more research is required to assess the accuracy of UTE-based QSM for trabecularized BM imaging.

Application and Main Findings

Relevant studies on the BMFF quantification at the spine using T_2* or QSM are shown in Table 2. In a recent study, T_2* and a T_2* ratio allowed for the discrimination between vertebral fractures of different origins, with a diagnostic accuracy of 73% and 89%, respectively, for distinguishing acute benign from malignant vertebral fractures.[76] While these values may not qualify the approach to be used independently, the T_2* and T_2* ratio may deliberately support diagnostics when combined with further dedicated anatomical sequences in the clinical setting. Regarding QSM, multiparametric trabecular bone R_2* mapping and QSM based on multi-echo gradient-echo imaging were shown to be feasible, with good sensitivity of QSM for measuring trabecular bone density in yellow BM regions.[78] In this context, R_2* represents the transverse, nonrecoverable relaxation rate, with R_2* = 1/T_2*. The decreases of calcium hydroxyapatite within vertebral bodies have been recently linked to increases in magnetic susceptibility values.[74,75,77] The first studies applying the technique showed significantly increased vertebral magnetic susceptibility in osteopenia and osteoporosis.[74,75,77] Furthermore, magnetic susceptibility was positively correlated with the proton density fat fraction (PDFF) as derived from CSE-MRI.[75] The sensitivity and specificity for differentiating osteoporosis from nonosteoporosis were 80.8% and 77.3%, respectively, and the area under the curve (AUC) for differentiating osteopenia from osteoporosis was significantly higher for the combination of magnetic susceptibility and PDFF than for PDFF alone.[74,75] Furthermore, QSM of the lumbar spine showed very good interobserver reliability and interscan reproducibility.[77] However, the studies on QSM referenced above employed methodologies that did not perform chemical shift encoding-based water–fat separation for generating the field map used in the magnetic susceptibility estimation and, therefore, their results should be primarily interpreted in a qualitative manner.[74,75,77]

TABLE 1. Overview of Major Advantages and Disadvantages of the Different Techniques Currently Applied to Quantitative Osteoporosis Imaging at the Spine and Femur, Including Information on the Basis of the Tissue Signal

Technique	Basis of tissue signal	Advantages	Disadvantages
High-resolution trabecular bone imaging	Resolving the trabecular bone matrix as signal void within the bone marrow signal.	- Direct depiction of trabecular bone matrix	- High spatial resolution requirement imposes long scanning times and results in sensitivity to motion - Not applicable for in vivo spine imaging due to the high sensitivity requirements
T_2* / Quantitative susceptibility mapping (QSM)	Indirect assessment of trabecular bone microstructure by exploiting magnetic susceptibility effects.	- High availability of multi-echo gradient-echo sequences for performing measurements - Moderate resolution can be adequate	- Indirect measurement of trabecular bone microstructure - T_2* mapping known to be affected by the anisotropic orientation of the trabecular bone microstructure - QSM requires an extensive processing pipeline and is still in early stages of validation
Ultrashort echo time (UTE) imaging	Bound and free water protons in bone are accessed by acquiring data at ultrashort echo times (<1 msec). Long T_2 tissue components are suppressed (eg, with an adiabatic inversion recovery pulse).	- Direct measurement of bone signal - Computed tomography-like image contrast for assessment of bone	- Low spatial resolution (due to rather long scanning times) - Low signal-to-noise ratio after long T_2 tissue component suppression
Magnetic resonance spectroscopy (MRS)	Water and fat signals can be differentiated based on their different chemical shift characteristics.	- High availability, implementation provided by the majority of available MRI systems - High spectral resolution - High robustness of water–fat signal identification - High accuracy and sensitivity, especially for low fat content - Possibility of characterization of mono-, di-, and polyunsaturated triglycerides	- Moderate scanning times - Limited spatial coverage or otherwise very long scanning times - Manual planning of a specific voxel of interest needed (requires trained operators) - Restrictions regarding the minimum required size for the voxel of interest - On-site expertise required for the processing of the acquired spectra
Chemical shift encoding-based water–fat imaging (CSE-MRI)	Water and fat signals are acquired simultaneously and are then separated according to a chemical shift encoding-based model.	- Moderate to high availability for modern MRI systems (thanks to common liver proton density fat fraction mapping applications) - High spatial resolution - High water–fat tissue signal contrast	- Consensus on optimized protocols for different B0 field strengths is still needed - Water–fat signal swap artifacts can arise from inaccurate B0 field map estimations

TABLE 1. Continued

Technique	Basis of tissue signal	Advantages	Disadvantages
		- High robustness of water–fat signal identification - High accuracy for proton density fat fraction definition after addressing confounding factors - Possibility of characterization of triglyceride composition (eg, number of double bonds or chain length, but requires prolonged scanning times) - Large spatial coverage in reasonable scanning times	

Ultrashort Echo Time Imaging

Background

In high-resolution imaging of trabecular bone, primarily applicable to the proximal femur, the signal voids are identified as bone due to the bone's low water content and short T_2 relaxation (Table 1). T_2* and QSM utilize the BM signal and the perturbance of such signal due to the susceptibility differences between trabecular bone and BM.[42,72,79–81]

Technical Principles

Another approach besides T_2* and QSM is the direct measurement of the bone matrix signal. The direct detection of the bone tissue signal itself is a challenging task due to its extremely rapid signal decay, which precludes the depiction of bone structures with conventional MRI sequences with TEs of 2–10 msec. Several MRI sequences were introduced with radial *k*-space sampling that allow the sampling at an UTE of 30–200 μs, which can enable the direct visualization of trabecular and cortical bone.[82–84] Cortical bone consists of ~40% mineral, 35% collagen, and 25% water by volume.[36] The short T_2 component detected by UTE imaging is predominantly from bound water and is in the range of 0.42–0.50 msec.[84,85]

The visualization of trabecular bone is limited by the presence of high signals from long-T_2 water and fat and due to the much lower proton density of trabecular bone. The suppression of long-T_2 tissues is critical for trabecular bone imaging and to achieve a desirable high contrast. Several methods for long-T_2 suppression have been proposed: dual-echo subtraction methods,[86–88] water–fat saturation techniques,[89,90] and long-T_2 suppression techniques based on inversion recovery (IR).[91–93] All of the presented approaches are suitable to generate contrast between long-T_2 and short-T_2 tissues. However, IR approaches can be designed to be time-efficient by combining a short TR and a turbo field echo readout.[91,94] Therefore, the inversion pulses are applied with a TR < T_1, leading to a quasi-steady-state of longitudinal magnetization. The z-magnetization of water in the steady-state is low due to its relatively long T_1, as compared to bone, yielding a contrast between water and bone signal. To eliminate the signal from fat, the UTE acquisition starts at the null point of the fat signal. A reduction of scan time is achieved when several readouts near the null point are acquired. Signal suppression is still possible, since excited signals before the null point and after the null point are of opposite polarity and since the data acquisition starts in the center of *k*-space for each readout. During the gridding process the signals from fat with opposite polarity, acquired before and after the null point of fat, annul each other.[91]

Application and Main Findings

In principal, UTE imaging in combination with long-T_2 suppression is a promising novel approach to visualize bone and to measure trabecular bone density directly (Fig. 3). It was recently shown that adiabatic IR-prepared UTE imaging in combination with a calibration phantom yields the trabecular bone proton density.[93] Specifically, using a hip agarose bone phantom and measurements in healthy subjects, it was demonstrated that high-contrast imaging of trabecular bone can be achieved ex vivo and in vivo (with fitted T_2* values of 0.3–0.45 msec and proton densities of 5–9 mol/L), suggesting the applicability of both selective imaging and quantitative assessment of short-T_2 water components in trabecular bone.[93] However, IR-prepared UTE sequences often have long scan times and the clinical value of this technique needs to be investigated further for application at the spine or femur. However, UTE imaging has been used ex vivo for

TABLE 2. Studies Using T_2* or Quantitative Susceptibility Mapping (QSM) for Quantification of the Bone Marrow Fat Fraction (BMFF) at the Spine

Author	Year	Cohort	Sequence/parameters	Main findings
Chen et al[74]	2018	70 postmenopausal women (mean age: 59 years) • 18 women with normal bone density • 26 women with osteopenia • 26 women with osteoporosis	QSM: • 3T • FOV: lumbar spine • multiecho(4 echoes) • TR/TE_1/TE_2/TE_3/TE_4: 20/0.1/2.4/4.6/6.8 msec	- QSM value showed to be significantly age-related and was significantly higher in patients with osteoporosis compared to patients with osteopenia or normal subjects. - The AUC, sensitivity, and specificity for differentiating osteopenia from nonosteopenia were 0.88, 86.5%, and 77.8%. - The AUC, sensitivity, and specificity for differentiating osteoporosis from nonosteoporosis were 0.86, 80.8% and 77.3%.
Guo et al[75]	2018	99 postmenopausal women (mean age: 58 years) • 26 women with normal bone density • 48 women with osteopenia • 25 women with osteoporosis	- CSE-MRI: • 3T • ROI: L1–L3 • multiecho(6 echoes) • TR/TE_1-TE_6: 5.6/1.0/1.7/2.4/3.1/3.8/4.5/5.2 msec - QSM: • 3T • FOV: lumbar spine • multiecho(4 echoes) • TR/TE_1/TE_2/TE_3/TE_4: 20/0.1/2.4/4.6/6.8 msec	- QSM value was significantly elevated in patients with osteopenia and osteoporosis when compared to normal subjects. - QSM value was significantly inversely correlated with BMD and significantly positively correlated with PDFF. - The AUC of the QSM value and PDFF was significantly higher than that of PDFF alone for differentiating between osteopenia and osteoporosis.
Schmeel et al[76]	2018	37 subjects (mean age: 65 years, 20 women), classification according to the entity of vertebral compression fractures: • 27 acute benign vertebral fractures • 25 malignant vertebral fractures	T_2*: • 3T • ROI: vertebrae with fractures / without fractures • multiecho(6 echoes) • TR/TE_1/ΔTE:8/1.2/1.2 msec	- T_2* and T_2* ratio (fracture T_2*/normal vertebrae T_2*) of malignant vertebral fractures were significantly higher compared to acute benign vertebral fractures (T_2*: 30 ± 11 vs. 19 ± 11 msec; T_2* ratio: 2.9 ± 1.6 vs. 1.2 ± 0.7). - AUC was 0.77 for T_2* and 0.88 for T_2* ratio, yielding a diagnostic accuracy of 73% and 89% for distinguishing acute benign from malignant vertebral fractures. - Root mean square absolute precision error was 0.44 msec as a measure for the T_2* short-term reproducibility.
Zhang et al[77]	2019	61 subjects (mean age: 56 years, 52 women) • 17 subjects with normal bone density	QSM: • 3T • FOV: lumbar spine	- QSM value and bone density showed good correlation in the L1–L4 vertebral bodies, especially in the L3 vertebral body.

TABLE 2. Continued

Author	Year	Cohort	Sequence/parameters	Main findings
		• 24 subjects with osteopenia • 20 subjects with osteoporosis	• multiecho(4 echoes) • $TR/TE_1/TE_2/TE_3/TE_4$: 20/0.1/2.4/4.6/6.8 msec	- QSM value showed excellent interobserver reliability and very good interscan reproducibility.

AUC = area under the curve; BMD = bone mineral density; BMFF = bone marrow fat fraction; CSE-MRI = chemical shift encoding-based water–fat MRI; FOV = field of view; PDFF = proton density fat fraction; QSM = quantitative susceptibility mapping; ROI = region of interest; TE = echo time; TR = repetition time.

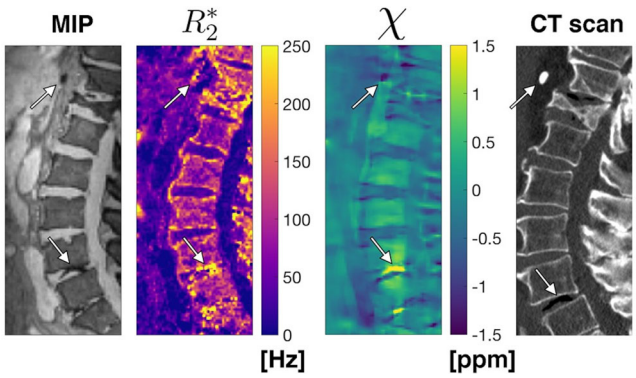

FIGURE 2: Quantitative susceptibility mapping (QSM) of the lumbar spine. Sagittal maximum intensity projection (MIP) over echo times (TEs), R_2*, susceptibility maps derived from chemical shift encoding-based water–fat magnetic resonance imaging (CSE-MRI) of the lumbar spine, and a corresponding scan by computed tomography (CT) are displayed. In this case, QSM is able to distinguish between a calcification and an air inclusion at the spine that similarly result in an increase of the transverse relaxation rate and in signal voids in the magnitude image. Sequence details (QSM): A time-interleaved multi-gradient-echo (TIMGRE) sequence with six echoes in two interleaves was acquired with the following parameters: $TR/TE_{min}/\Delta TE_{eff}$ = 9.9/1.33/1.1 msec, FOV = 220 × 220 × 80 mm^3, voxel size = 1.8 mm^3, flip angle = 3°.

valid cortical bone porosity assessment of the tibia, as well as in healthy subjects to investigate pore water concentration mapping of tibial cortical bone, for instance, thus pointing at potential clinical utility.[95,96]

Magnetic Resonance Spectroscopy

Background

To date, single-voxel proton MRS has been the most frequently applied technique for quantification of BM (Fig. 4). This technique acquires data from a prescribed localized volume of interest (VOI) with high spectral resolution. Thus, it enables the quantification of individual chemical components based on their resonance frequency, namely water and fat in the case of BM (Table 1).

Technical Principles

Both point-resolved spectroscopy (PRESS) and stimulated echo acquisition mode (STEAM) sequences were predominantly used. However, STEAM has relevant advantages over PRESS. It enables shorter minimum TEs and, thus, features higher signal for the short-T_2 water component of the BM spectrum despite its intrinsic signal loss of about 50% compared to PRESS. MRI-based quantification of fat of BM can be expressed as the BMFF, but most notably as the PDFF, which can be regarded as a fundamental tissue property and is defined as the ratio of density of mobile protons from fat (triglycerides) and the total density of protons from mobile triglycerides and mobile water.[97] Confounding relaxation effects have to be corrected for in order to quantify the PDFF. Measurements at multiple TEs have to be acquired at suitable TRs to allow for the correction of T_2-weighting and T_1-weighting effects, respectively. Regarding the placement of the VOI, it is important to take into account chemical shift displacement effects due to finite RF pulse bandwidths of the MRS sequence. At 3T, this can typically result in an offset of up to 15% of the voxel size in each spatial dimension between the water and fat localization.[98] To reduce this effect and subsequent quantification errors, the VOI should be placed with caution within the vertebral body or proximal femur to avoid severe inhomogeneities, degenerative changes including subchondral sclerosis, or vascular structures.

Application and Main Findings

Several studies have applied MRS for measuring the BMFF at the spine; fewer have investigated the proximal femur. The most relevant MRS studies are shown in Tables 3 and 4. Associations between the BMFF and BMD or T-scores have been demonstrated repeatedly at the level of the spine and proximal femur, respectively, with the BMFF being elevated in subjects with osteoporosis and negative correlations indicating an increase in the BMFF with BMD loss.[39,100–103,105,107,108,110,111,113] Griffith et al were among the first reporting elevated BMFF depending on the subjects' BMD,

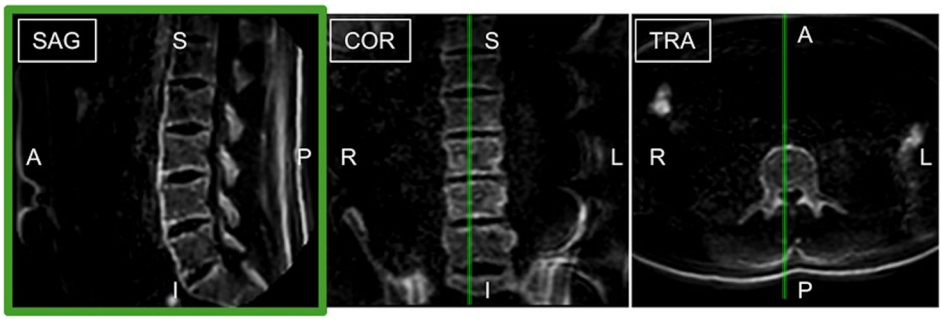

FIGURE 3: Ultrashort echo time (UTE) imaging of the lumbar spine. Imaging of the lower spine of a 29-year-old healthy male with a 3D inversion recovery (IR)-prepared UTE stack-of-stars sequence. The scan was acquired in sagittal plane with an isotropic resolution of 3 mm and reformatted subsequently to obtain the coronal and transversal images. Cortical bone, trabecular bone, and skin appeared bright; other soft tissues like fat and muscles were suppressed. Sequence details (IR-UTE stack-of-stars sequence): TR = 2.03 msec, TE = 0.14 msec, FOV = 250 × 250 × 300 mm^3, voxel size = 3.0 × 3.0 × 3.0 mm^3, receiver bandwidth = 3285 Hz/pixel, 1 average, flip angle = 16°. For the long T_2 suppression a trapezoidal adiabatic offset-independent inversion pulse was used, with an interval of 160 msec between two inversion pulses. The excitation and readout started after 55 msec when fat was nulled.

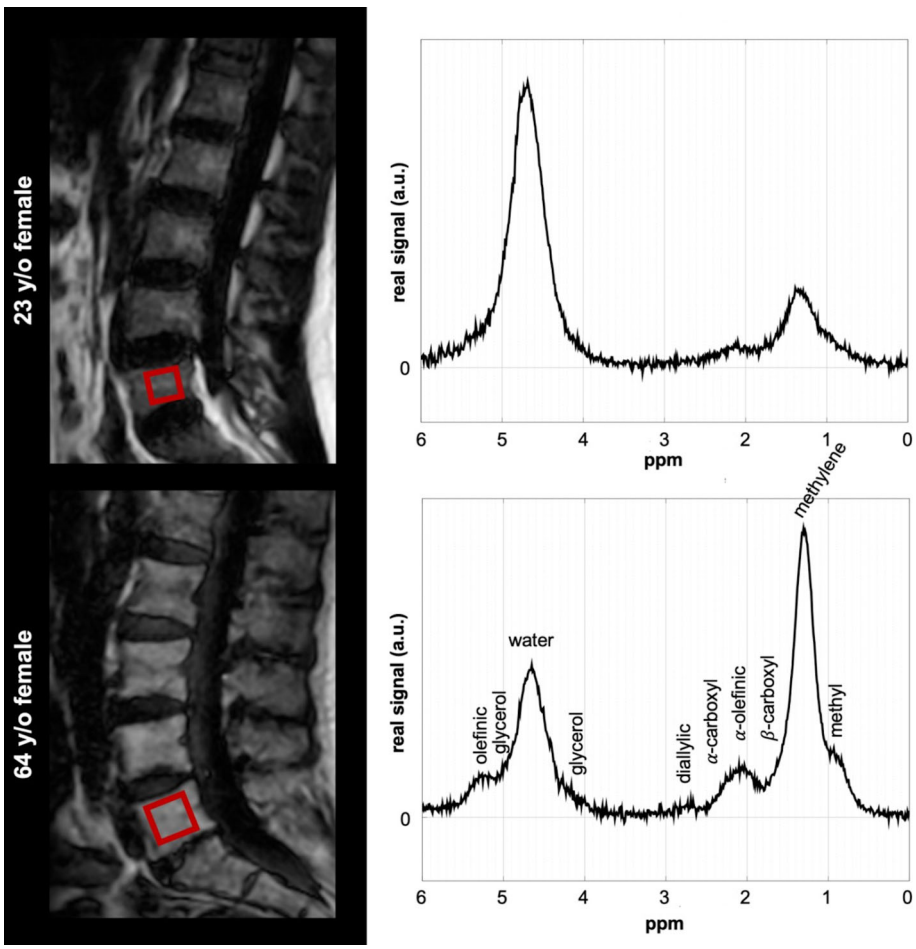

FIGURE 4: Magnetic resonance spectroscopy (MRS) of the lumbar spine. Fat images derived from a six-echo Dixon sequence of the lumbar spine and corresponding spectrums derived from single-voxel stimulated echo acquisition mode (STEAM) MRS of the L5 vertebral body for a 23-year-old female (upper row) and a 64-year-old female (lower row) are shown. A higher water peak and more broad linewidths are present in the younger subject. Red boxes indicate the voxel of interest (VOI) placements for MRS. Characteristic triacylglycerol peaks were labeled in the spectrum of the older subject. Sequence details (STEAM MRS): TR = 6 sec, TE = 11 msec, TM = 16 msec, 8 averages in 4 phase cycles, 4096 samples, spectral bandwidth = 5000 Hz, voxel size = 15 mm^3.

using MRS at 1.5T in 82 men and 103 women at the level of the lumbar spine.[39,101] In detail, the vertebral BMFF was significantly increased in both elderly men and women with osteoporosis (males: 58.2 ± 7.8%, females: 67.8 ± 8.5%) as compared to subjects with normal BMD values (males: 50.5 ± 8.7%, females: 59.2 ± 10.0%).[39,101] Analogously,

TABLE 3. Studies Using Magnetic Resonance Spectroscopy (MRS) for Quantification of the Bone Marrow Fat Fraction (BMFF) at the Spine

Author	Year	Cohort	Sequence/parameters	Main findings
Kugel et al[99]	2001	154 healthy subjects (84 women), categorized according to age: • age range 11–20 years: 15 subjects • age range 21–30 years: 39 subjects • age range 31–40 years: 42 subjects • age range 41–50 years: 23 subjects • age range 51–60 years: 17 subjects • age ≥ 61 years: 18 subjects	MRS: • 1.5T • VOI: L3 • PRESS • TR/TE: 2000/40 msec	- BMFF increases with age from 24% (11–20 years) to 54% (≥61 years). - BMFF in women is less than that in male subjects in the same age group.
Griffith et al[39]	2005	82 men (mean age: 73 years): • 42 men with normal bone density • 23 men with osteopenia • 17 men with osteoporosis	MRS: • 1.5T • VOI: L3 • PRESS • TR/TE: 3000/25 msec	BMFF was significantly increased in osteoporotic and osteopenic subjects compared to normal subjects.
Yeung et al[100]	2005	- 50 women (mean age: 70 years): • 15 women with normal bone density • 15 women with osteopenia • 20 women with osteoporosis - 12 young women as control subjects (mean age: 28 years)	MRS: • 1.5T • VOI: L3 • PRESS • TR/TE: 3000/25 msec	- BMFF was significantly elevated in osteoporotic and osteopenic subjects compared to normal subjects and young controls. - Fat unsaturation index was significantly decreased in osteoporotic and osteopenic subjects compared to normal subjects and young controls.
Griffith et al[101]	2006	103 women (mean age: 72 years): • 18 women with normal bone density • 30 women with osteopenia • 55 women with osteoporosis	MRS: • 1.5T • VOI: L3 • PRESS • TR/TE: 3000/25 msec	BMFF was significantly increased in osteoporotic subjects compared to normal subjects.
Li et al[102]	2011	- 38 women with osteopenia or osteoporosis (mean age: 62 years) - 13 women with normal bone density as control subjects (mean age: 57 years)	MRS: • 3T • VOI: L1–L4 • PRESS • TR/TE: 3000/37 msec	- BMFF significantly increased from L1 to L4. - BMFF was significantly elevated in patients with osteoporosis/osteopenia compared to normal subjects. - Average coefficient of variation of BMFF quantification was 1.7%.

TABLE 3. Continued

Author	Year	Cohort	Sequence/parameters	Main findings
Baum et al[103]	2012	- 13 women with diabetes (mean age: 59 years) - 13 women without diabetes as control subjects (mean age: 57 years)	MRS: • 3T • VOI: L1–L3 • PRESS • TR/TE: 3000/37 msec	- BMFF was significantly inversely correlated with BMD in the whole study population. - Mean BMFF was similar in diabetic women and healthy controls, mean unsaturated lipid levels were significantly lower in the diabetic group. - Subcutaneous and total adipose tissue correlated significantly with the mean BMFF in the whole study population - Significant correlations of the mean BMFF with visceral adipose tissue and HbA1c were observed only in the diabetic group.
Patsch et al[104]	2013	69 women (mean age: 63 years): • 33 women without vertebral fractures, 16 of them diagnosed with diabetes • 36 women with vertebral fragility fractures, 17 of them diagnosed with diabetes	MRS: • 3T • VOI: L1–L3 • PRESS • TR/TE: 3000/37 msec	- The prevalence of vertebral fragility fractures was significantly associated with −1.7% lower unsaturation levels and +2.9% higher saturation levels. - Diabetes was associated with −1.3% lower unsaturation and +3.3% higher saturation levels. - Diabetic subjects with fractures had the lowest marrow unsaturation and highest saturation.
Schwartz et al[105]	2013	257 subjects (mean age: 79 years, 139 women): • 204 subjects without prevalent vertebral fractures (previous fractures not excluded) • 21 men with prevalent vertebral fractures • 32 women with prevalent vertebral fractures	MRS: • 1.5T • VOI: L1–L4 • PRESS • TR/TE: 2000/37 msec	- Subjects with prevalent vertebral fractures had higher BMFF, with a significant difference only in men. - BMFF was associated with lower trabecular volumetric BMD but not with cortical volumetric BMD in women. -Areal BMD was negatively correlated with BMFF in women only.
Cohen et al[106]	2015	- 9 women with osteoporosis (mean age: 35 years) - 7 women with normal bone density as control subjects (mean age: 37 years)	MRS: • 1.5T • VOI: L3 (and intertrochanteric region) • PRESS • TR/TE: 3000/25 msec	- Lumbar BMFF correlated significantly with marrow fat variables on iliac crest biopsies. - Marrow fat quantity was greater at the femur than at L3 and the iliac crest and correlated inversely with total hip and femoral neck BMD.
Karampinos et al[107]	2015	10 vertebrae (between T5–T10) from 4 human cadavers (mean age: 58 years, 1 woman)	MRS: • 3T • VOI: harvested vertebrae • STEAM • TR/TE_1-TE_4: 6 s/12/15/20/25 msec	- BMFF showed significant negative correlations to BMD and FL. - FL showed strong significant correlations with BMD and trabecular microstructure parameters.

TABLE 3. Continued

Author	Year	Cohort	Sequence/parameters	Main findings
Sheu et al[108]	2017	156 men (mean age: 81 years): • 118 men without diabetes • 38 men diagnosed with diabetes	MRS: • 3T • VOI: L1–L3 • PRESS • TR/TE: 3000/37 msec	- Men with diabetes had a significantly higher spine BMFF and BMD than those without diabetes. - BMFF showed significant inverse associations to BMD among diabetic men, but not in nondiabetic men.
Mistry et al[109]	2018	470 subjects (mean age: 82 years), categorized according to gender: • 226 women • 244 men	MRS: • 1.5T • VOI: L1–L4 • PRESS • TR/TE: n.a.	- Per 1 pg/ml increase in total estradiol, there was a significant decrease in BMFF in men and a nonsignificant decrease in women, with no evidence of interaction by gender. - Per 10 ng/dl increase in total testosterone, there was a significant decrease in BMFF in men and a nonsignificant decrease in women, with no evidence of interaction by gender.
He et al[110]	2019	123 subjects (mean age: 56 years, 73 women): • 27 women / 22 men with normal bone density • 21 women / 17 men with osteopenia • 25 women / 11 men with osteoporosis	MRS: • 3T • VOI: L2–L4 • PRESS • TR/TE: 3000/30 msec	- BMFF increased with decreasing BMD in both women and men. - There were significant sex differences in BMFF among subjects with normal bone density. - BMFF was significantly negatively correlated with BMD in all subjects.

BMD = bone mineral density; BMFF = bone marrow fat fraction; FL = failure load; MRS = magnetic resonance spectroscopy; PRESS = point-resolved spectroscopy; STEAM = stimulated echo acquisition mode; TE = echo time; TR = repetition time; VOI = voxel of interest.

Griffith et al used MRS at 1.5T with VOIs placed in the femoral head, neck, and subtrochanteric region of the femoral shaft, reporting on significant BMFF increases with decreased BMD for these locations among a cohort of 120 elderly women.[111] At the femoral neck, the BMFF amounted to 80.8 ± 9.4% in normal subjects, whereas it was 86.2 ± 6.5% in osteopenic and 88.4 ± 4.8% in osteoporotic subjects, respectively.[111]

At the spine, increased BMFF and decreased BMD have also been related to biomechanical properties: an in vitro study harvested vertebrae from human cadavers and demonstrated a significant negative correlation between the BMFF and the biomechanical failure load.[107] Other studies reported on the BMFF being positively associated with prevalent vertebral fractures in men and on fat unsaturation levels being negatively associated with the prevalence of fragility fractures.[104,105] Generally, fat unsaturation levels were reported to be decreased in osteoporotic subjects, as well as in diabetic subjects, and were proposed as complementary imaging biomarkers to assess fracture risk, especially in subjects with increased fracture risk despite regular BMD, such as in type 2 diabetes mellitus.[100,103,104]

For the femoral neck, a combined approach using MRS and diffusion tensor imaging (DTI) was described to be sensitive and specific in identifying osteoporotic subjects, with a positive correlation being reported for fractional anisotropy (FA) and BMFF in osteopenic and/or osteoporotic subjects.[112,113] Regarding the femoral neck of elderly women, methylene, glycerol, and total lipid resonances were significantly lower in healthy as compared to osteoporotic subjects, and significant correlations were revealed between total lipids and the T-score, respectively.[114]

Vertebral BMFF was reported to be dependent on age and gender, and it shows anatomical variations.[99,102,103,109] Subcutaneous adipose tissue (SAT) volume and total adipose tissue volume correlated significantly with the BMFF in females with and without diabetes, while significant

TABLE 4. Studies Using Magnetic Resonance Spectroscopy (MRS) for Quantification of the Bone Marrow Fat Fraction (BMFF) at the Proximal Femur

Author	Year	Cohort	Sequence/parameters	Main findings
Griffith et al[111]	2008	120 women (mean age. 74 years): • 39 women with normal bone density • 47 women with osteopenia • 34 women with osteoporosis	MRS: • 1.5T • VOI: femoral head, neck, and subtrochanteric region of the femoral shaft • PRESS • TR/TE: 3000/ 25 msec	- BMFF increases with decreased BMD in the femoral head, femoral neck, and femoral shaft. - Subjects with osteoporosis had significantly higher BMFF in the femoral head, femoral neck, and femoral shaft compared to subjects with normal bone density. - Subjects with osteopenia had significantly higher BMFF in the femoral neck and femoral shaft compared to subjects with normal bone density.
Manenti et al[112]	2013	20 women (mean age: 72 years), categorized as healthy, osteopenic, or osteoporotic (single group sizes not provided)	MRS: • 3T • VOI: femoral neck • PRESS • TR/TE: 4000/ 28 msec	- BMFF can discriminate healthy and osteoporotic subjects. - MD and FA as derived from additional DTI can discriminate healthy subjects from osteopenic and osteoporotic subjects. - MD/BMFF vs. FA/BMFF graphs can identify all healthy subjects.
Manenti et al[113]	2013	40 women (mean age: 69 years): • 12 women with normal bone density • 14 women with osteopenia • 14 women with osteoporosis	MRS: • 3T • VOI: femoral neck • PRESS • TR/TE: 4000/ 28 msec	- BMFF was significantly different between healthy and osteoporotic subjects only. - Significant correlations between BMFF and T-score and between BMFF and age were observed for the whole cohort. - A significant positive correlation between FA as derived from additional DTI and BMFF was found in osteopenic and osteoporotic subjects, but not in healthy subjects (where a significant correlation between MD and BMFF was found).
Cohen et al[106]	2015	- 9 women with osteoporosis (mean age: 35 years) - 7 women with normal bone density as control subjects (mean age: 37 years)	MRS: • 1.5T • VOI: intertrochanteric region (and L3) • PRESS • TR/TE: 3000/ 25 msec	- There were no significant correlations between BMFF at the femur and marrow fat on biopsies (in contrast to findings for the lumbar spine). - Marrow fat quantity was greater at the femur than at L3 and the iliac crest and correlated inversely with total hip and femoral neck BMD.
Di Pietro et al[114]	2016	- 33 women (mean age: 68 years): • 11 women with normal bone density • 12 women with osteopenia	MRS: • 3T • VOI: femoral neck • PRESS	- Methylene (L13), glycerol (L41, L43), and total lipid resonances were significantly lower in healthy

TABLE 4. Continued

Author	Year	Cohort	Sequence/parameters	Main findings
		• 10 women with osteoporosis	• TR/TE: 4000/ 28 msec	as compared to osteoporotic subjects. - A significant negative correlation was found between total lipids and the T-score, and a significant positive correlation was found between water and the T-score.

BMD = bone mineral density; BMFF = bone marrow fat fraction; DTI = diffusion tensor imaging; FA = fractional anisotropy; MD = mean diffusivity; MRS = magnetic resonance spectroscopy; PRESS = point-resolved spectroscopy; TE = echo time; TR = repetition time; VOI = voxel of interest.

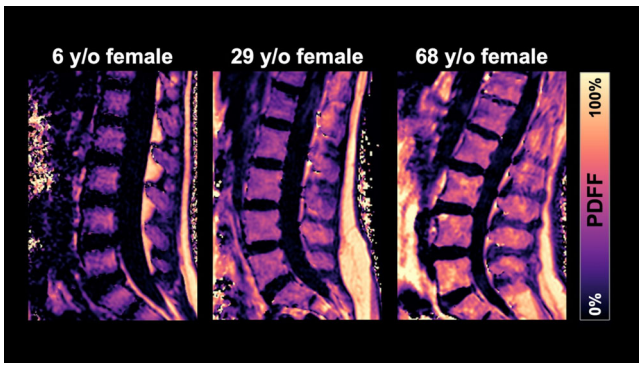

FIGURE 5: Chemical shift encoding-based water–fat magnetic resonance imaging (CSE-MRI) of the lumbar spine. Sagittal proton density fat fraction (PDFF) maps derived from CSE-MRI of the lumbar spine in a 6-year-old girl, 29-year-old female, and 68-year-old female are displayed. Increases in the PDFF are shown with age and in the craniocaudal direction from L1 to L5 vertebral bodies, respectively. Sequence details (CSE-MRI): 6-year-old girl: Time-interleaved multi-gradient-echo (TIMGRE) sequence with two interleaved repetition times (TRs) acquiring three echoes using fly-back and constant effective echo spacing: TR = 8.8–12.9 msec, effective TE spacing = 1.2–1.3 msec, first TE = 1.5–1.7 msec, 16–26 sagittal slices with a slice thickness of 1.2–3 mm, S/I and A/P FOV = 360–500 and 140–240 mm, voxel resolution = 1.2–1.6 mm, flip angle = 3°. 29-year-old female and 68-year-old female: 3D spoiled gradient-echo sequence with eight echoes in a single TR using non-fly-back gradients: TR/TE$_1$/ΔTE = 11/1.4/1.1 msec, FOV = 220 × 220 × 80 mm^3, acquisition matrix = 124 × 121, voxel size = 1.8 × 1.8 × 4.0 mm^3, receiver bandwidth = 1527 Hz/pixel, frequency direction = A/P, flip angle = 3°.

correlations of the BMFF with visceral adipose tissue (VAT) and HbA1c, the most important blood marker for diabetes, were observed only in diabetic females.[103] Vertebral BMFF was higher in men as compared to women; however, this has been observed among healthy subjects and not explicitly in subjects with osteoporosis.[99] Furthermore, the BMFF shows an increase from the L1 to L4 vertebral bodies in subjects with low BMD, indicating anatomical variations at the spine.[102] Lastly, BMFF measured at the L3 vertebral body was significantly associated with BM parameters on iliac crest biopsies, which was not the case for BMFF measured at the intertrochanteric region.[106] The reproducibility of the MRS-based BMFF measurements at the spine, reported in terms of the coefficient of variation, was determined to be equal to 1.7%.[102]

Chemical Shift Enconding-Based Water–Fat Imaging

Background

Assessment by CSE-MRI allows spatially resolved quantification of the BMFF (Fig. 5). Sequences typically used at 3T include bipolar gradient readout sequences acquiring all echoes (usually six echoes) within a single TR and monopolar time-interleaved gradient echo sequences where all echoes (usually six echoes) are acquired in multiple TRs (Table 1). At 1.5T, nontime-interleaved monopolar readouts acquiring all echoes in a single TR are also used.[115]

Technical Principles

For fat quantification, complex- or magnitude-based parameter estimations were conducted.[115–117] While complex-based techniques have shown superiority to magnitude-based approaches due to lower sensitivity to fat signal modeling errors and better noise performance, they are nevertheless prone to phase errors. In addition, T_1 bias and T_2* decay effects need to be considered in order to extract the PDFF.[115,116,118–120] These effects can introduce considerable bias during BMFF measurements, thus requiring an appropriate selection of experimental parameters; for example, small flip angles to reduce T_1 bias, and d1istinct correction of T_2* decay effects during the postprocessing stage.[115,121–123] Compared to applications of the PDFF in other organs, T_2* decay effects have to be considered in particular when measuring the PDFF in the presence of trabecular bone, which shows

TABLE 5. Studies Using Chemical Shift Encoding-Based Water–Fat Magnetic Resonance Imaging (CSE-MRI) for Quantification of the Bone Marrow Fat Fraction (BMFF) at the Spine

Author	Year	Cohort	Sequence/parameters	Main findings
Kühn et al[81]	2013	51 subjects (mean age: 70 years, 28 women): • 92 vertebral bodies with normal bone density • 47 vertebral bodies with osteopenia • 34 vertebral bodies with osteoporosis	CSE-MRI: • 3T • ROI: L1–L5 • multiecho(3 echoes) • TR/TE_1/TE_2/TE_3: 6.5/1.2/2.5/4.9 msec	- PDFF was significantly increased in osteoporosis compared with healthy subjects. - R_2* with correction for multiple-peak fat showed significant differences between normal and osteopenia and between normal and osteoporosis.
Baum et al[124]	2015	28 healthy subjects (mean age: 26 years, 11 women)	CSE-MRI: • 3T • ROI: C3–L5 • multiecho(8 echoes) • TR/TE_{min}/ΔTE: 15/1.5/1.1 msec	- PDFF significantly increased from C3 to L5. - The repeatability for PDFF measurements, averaged over C3–L5, expressed as absolute precision error was 1.7%.
Baum et al[125]	2018	156 healthy subjects, categorized according to age: • age range 20–29 years (twenties): 12/30 males/females • age range 30–39 years (thirties): 15/9 males/females • age range 40–49 years (forties): 4/14 males/females • age range 50–59 years (fifties): 9/27 males/females • age range 60–69 years (sixties): 5/19 males/females • age range 70–79 years (seventies): 4/8 males/females	CSE-MRI: • 3T • ROI: L1–L4 • multiecho(8 echoes) • TR/TE_1/ΔTE: 11/1.4/1.1 msec	- PDFF was significantly higher in males than females in the twenties and thirties. - With increasing age, females showed an accelerated fatty conversion with no significant PDFF differences in the forties and fifties. - The accelerated conversion process continued with age, resulting in greater PDFF in females than males in the sixties and seventies. - Relative age-related PDFF change from the twenties to the seventies increased from 16.7% (L1) to 51.4% (L4) in males and 76.8% (L1) to 85.7% (L4) in females.
Schmeel et al[126]	2018	57 subjects (mean age: 67 years, 29 women), classification according to the entity of vertebral compression fractures: • 46 acute benign vertebral fractures • 41 malignant vertebral fractures	CSE-MRI: • 3T • ROI: vertebrae with fractures / without fractures • multiecho(6 echoes) • TR/TE_1/TEspacing: 8/1.2/1.2 msec	- PDFF and PDFF ratio (fracture PDFF/normal vertebrae PDFF) of malignant vertebral fractures were significantly lower compared to acute benign vertebral fractures (PDFF: 3.48 ± 3.30% vs. 23.99 ± 11.86%; PDFF ratio: 0.09 ± 0.09 vs. 0.49 ± 0.24). - AUC was 0.98 for PDFF and 0.97 for PDFF ratio, with a corresponding accuracy of 96% and 95% for differentiating between acute benign and malignant vertebral fractures. - PDFF remained the only imaging-based variable to independently differentiate between acute benign and

TABLE 5. Continued

Author	Year	Cohort	Sequence/parameters	Main findings
				malignant vertebral fractures (OR: 0.454).
Schmeel et al[127]	2018	66 subjects (mean age: 65 years, 36 women), classification according to the entity of vertebral lesions: • 77 benign vertebral lesions • 44 malignant vertebral lesions	CSE-MRI: • 3T • ROI: vertebrae with lesions / without lesions • multiecho(6 echoes) • TR/TE_1/TEspacing: 8/1.2/1.2 msec	- PDFF of malignant lesions was statistically significantly lower in comparison with benign lesions and normal vertebral bone marrow. - AUC was 0.97 for differentiating benign from malignant lesions and 0.95 for differentiating acute vertebral fractures from malignant lesions, yielding a diagnostic accuracy of 96% in the differentiation of both benign lesions and acute vertebral fractures from malignancy.
Sollmann et al[128]	2018	39 women, categorized according to age / menopausal status: • 15 premenopausal women (mean age: 30 years) • 24 postmenopausal women (mean age: 63 years)	CSE-MRI: • 3T • ROI: L1–L5 (and in erector spinae muscles) • multiecho(6 echoes) • TR/TE/ΔTE: 6.4/1.1/0.8 msec	- PDFF of the paraspinal musculature and bone marrow were significantly lower in premenopausal women when compared to postmenopausal women. - A significant correlation was shown in postmenopausal, but not premenopausal women between the PDFF of the erector spinae muscles and the PDFF of the vertebral bone marrow.
Burian et al[129]	2019	41 women, categorized according to age / menopausal status: • 15 premenopausal women (mean age: 30 years) • 26 postmenopausal women (mean age: 65 years)	CSE-MRI: • 3T • ROI: L1–L5 • multiecho (8 echoes) • TR/TE_1/ΔTE: 11.0 /1.4/1.1 msec	- PDFF was significantly lower in premenopausal women when compared to postmenopausal women. - PDFF increased from L1 (37.9%) to L5 (45.2%). - Bone marrow heterogeneity based on texture analysis was significantly increased in postmenopausal women. - Contrast and dissimilarity performed best in differentiating pre- and postmenopausal women (AUC = 0.97 and 0.96), but not significantly different when compared to PDFF (AUC = 0.97).
Zhao et al[130]	2019	257 subjects (mean age: 49 years, 181 women) • 74 women / 61 men with normal bone density • 70 women / 12 men with osteopenia	CSE-MRI: • 3T • ROI: L1–L3 • multiecho(6 echoes) • TR/TE_1/ΔTE: 5.6/1.0/0.7 msec	- Moderate inverse correlations were found between BMFF and BMD. - The AUC, sensitivity, specificity, and NPV for predicting subjects with osteoporosis were 0.896,

TABLE 5. Continued

Author	Year	Cohort	Sequence/parameters	Main findings
		• 37 women / 3 men with osteoporosis		0.848, 0.853, and 0.969, respectively.

AUC = area under the curve; BMD = bone mineral density; BMFF = bone marrow fat fraction; CSE-MRI = chemical shift encoding-based water–fat MRI; NPV = negative predictive value; OR = odds ratio; PDFF = proton density fat fraction; ROI = region of interest; TE = echo time; TR = repetition time.

reduced T_2* relaxation values due to microscopic magnetic field inhomogeneity effects.

Application and Main Findings

Relevant studies on the BMFF quantification using CSE-MRI are shown in Tables 5 and 6. As for MRS, the majority of studies investigated the spine, with fewer studies performing CSE-MRI at the proximal femur. Importantly, good agreement has been reported between MRS-based BMFF quantification as the gold-standard method and CSE-MRI-based BMFF quantification for the spine as well as the proximal femur.[131–134] At the spine, the BMFF derived from CSE-MRI showed increased values in subjects with osteoporosis and inverse correlations with BMD and T-scores.[81,130,132] The reproducibility of BMFF measurements, expressed as an absolute precision error for the PDFF, has been reported in the range of 1.70% (C3 to L5 vertebral bodies) and 1.45% (L1 to L4 vertebral bodies).[124,132] Along the spinal axis, the BMFF showed an increase in the craniocaudal direction.[124,129] Specifically, as derived from measurements from C3 to L5, segment-specific differences in measurements between males and females have been reported, with the BMFF averaged over C3–C7, T1–T6, T7–T12, and L1–L5 vertebral bodies in young, healthy men and women (mean age: 26 years) amounting to 31.7 ± 7.9% and 23.0 ± 7.8%, 33.8 ± 6.8% and 24.6 ± 8.8%, 33.8 ± 6.4% and 26.1 ± 6.4%, and 38.8 ± 7.6% and 31.5 ± 12.4%, respectively.[124] In children, cervical, thoracic, and lumbar BMFF measurements were significantly associated with the natural logarithm of age, with differences in the BMFF between boys and girls being not yet significant.[133] At the proximal femur, subregion-specific significant differences in fat composition in postmenopausal compared to premenopausal women were observed, with postmenopausal women demonstrating higher saturation (+14.7% to +43.3%), but lower mono- (−11.4% to −33%) and polyunsaturation (−52% to −83%).[135] Specifically, within red marrow adipose tissue, postmenopausal women showed lower fat content (−16% to −24%) and decreased polyunsaturation (−80% to −120%) in the femoral neck, greater trochanter, and Ward's triangle.[135]

An accelerated fatty conversion of BM was observed in women as compared to men with increasing age, particularly evident after the menopause.[125] Of note, significant correlations between fat fractions of paraspinal and vertebral BM compartments were observed recently in postmenopausal women, thus potentially providing a hint for direct associations between vertebrae and other body fat compartments.[128] Furthermore, in postmenopausal women BM heterogeneity as evaluated by means of texture analysis based on CSE-MRI was significantly increased at the spine.[129] Among the parameters estimated using gray-level co-occurrence matrix analysis, contrast and dissimilarity performed best in differentiating pre- and postmenopausal women.[129]

The PDFF derived from CSE-MRI has recently been shown to facilitate discrimination between benign osteoporotic and malignant vertebral fractures, which can be challenging in the acute clinical setting.[126,127] The PDFF of vertebral BM and a PDFF ratio (fracture PDFF divided by normal vertebrae PDFF) were significantly lower in malignant vertebral compression fractures when compared to acute osteoporotic fractures (PDFF: 3.48 ± 3.30% vs. 23.99 ± 11.86%; PDFF ratio: 0.09 ± 0.09 vs. 0.49 ± 0.24).[126] Moreover, the diagnostic accuracy was 96% regarding the differentiation of benign lesions and acute vertebral fractures from malignancy.[127] Acute vertebral fractures showed an average PDFF that was clearly higher than those of malignant tumors like vertebral metastases, multiple myeloma, and chordoma, while being lower than the PDFF of hemangioma or degenerative changes of vertebral endplates.[127]

Multidimensional Investigation and Parametric Mapping

Background

Regarding region-specific interactions, there is a lack of knowledge concerning the 3D spatial interrelationships between BMFF and BMD. However, investigations of such spatial associations could improve our understanding of bone fragility in critical anatomical regions like the proximal femur. Statistical parametric mapping (SPM) is an advanced image analysis technique with a framework that enables this type of spatial assessment.[136]

Technical Principles

SPM is a computational anatomy technique where voxel-based (volumetric) or vertex-based (surface) maps of tissue

TABLE 6. Studies Using Both Magnetic Resonance Spectroscopy (MRS) and Chemical Shift Encoding-based Water–Fat Magnetic Resonance Imaging (CSE-MRI) for Quantification of the Bone Marrow Fat Fraction (BMFF) at the Spine or Proximal Femur

Author	Year	Cohort	Sequence/parameters	Main findings
Shen et al[131]	2013	27 healthy, postmenopausal women (mean age: 55 years)	- MRS: • 1.5T • VOI: L3 • PRESS • TR/TE: 3000/25 msec - CSE-MRI: • 1.5T • ROI: L3 and femoral neck • dual-echo • TR/TE: 150/2.1 and 4.4 msec	- High correlations were found between MRS, CSE-MRI, and/or T_1-weighted imaging regarding bone marrow adipose tissue: correlations ranged from 0.78 to 0.88 in the L3 vertebra and the correlation was 0.86 in femoral necks. - The inhomogeneous distribution of bone marrow fat, the threshold segmentation of the T_1-weighted MRI, and the ambiguity of the CSE-MRI may reflect reasons for the difference among methods.
Li et al[132]	2017	83 postmenopausal women (mean age: 63 years) • 41 women with normal bone density • 26 women with osteopenia • 16 women with osteoporosis	- MRS: • 3T • VOI: L3 • STEAM • TR/TE_1/TE_2/TE_3/TE_4: 6000/11/15/20/25 msec - CSE-MRI: • 3T • ROI: L1–L4 • multiecho(8 echoes) • TR/TEinit/ΔTE: 10/1.5/1.2 msec	- High correlations were found between MRS and CSE-MRI regarding BMFF. - The intra- and interrater agreements for BMFF as measured by CSE-MRI were excellent. - The repeatability for BMFF of CSE-MRI expressed as absolute precision error was 1.45%. - Inverse correlations showed to be considerably similar between BMD, T-score, and CSE-based BMFF or MRS-based BMFF even when controlling for age, years since menopause, and BMI.
Ruschke et al[133]	2017	93 subjects (median age: 4.5 years, range: 0.1–17.6 years, 49 females and 44 males)	- MRS: • 3T • VOI: L4 • STEAM • TR/TE_1/TE_2/TE_3/TE_4: 5000/12/16/20/24 msec - CSE-MRI: • 3T • ROI: C3–L5 • multiecho(6 echoes) • TR/TEspacing/TE_1: 8.8–12.9/1.2–1.3/1.5–1.7 msec	- High correlations were found between MRS and CSE-MRI regarding PDFF. - Cervical, thoracic, and lumbar PDFF correlated significantly with the natural logarithm of age.

TABLE 6. Continued

Author	Year	Cohort	Sequence/parameters	Main findings
Martel et al[134]	2019	31 subjects, categorized according to the presence of either idiopathic osteoporosis or glucocorticoid-induced osteoporosis: • 18 women with (idiopathic) osteoporosis (mean age: 53 years) • 13 women with glucocorticoid-induced osteoporosis (mean age: 38 years)	- MRS: • 3T • VOI: femoral neck and Ward's triangle • STEAM • TR/TE:2500/20 msec - CSE-MRI: • 3T • ROI: femoral head, femoral neck, Wards triangle, greater trochanter • multiecho(12 echoes) • $TR/TE_{1\text{-}12}$: 16/(1:12) × 1.2 msec	- Subjects with glucocorticoid-induced osteoporosis compared with subjects with (idiopathic) osteoporosis showed decreased monounsaturated fat fraction in the femoral head as well as decreased monounsaturated fat fraction, increased saturated fat fraction, and decreased T_2* in the femoral neck. - Furthermore, subjects with glucocorticoid-induced osteoporosis presented with decreased PDFF, monounsaturated fat fraction, polyunsaturated fat fraction, increased saturated fat fraction, and decreased T_2* in the femoral triangle. - There was high measurement agreement between CSE-MRI and MRS using the Bland–Altman test.

BMD = bone mineral density; BMFF = bone marrow fat fraction; BMI = body mass index; CSE-MRI = chemical shift encoding-based water–fat MRI; MRS = magnetic resonance spectroscopy; PDFF = proton density fat fraction; PRESS = point-resolved spectroscopy; ROI = region of interest; STEAM = stimulated echo acquisition mode; TE = echo time; TR = repetition time; VOI = voxel of interest.

parameters in a population (eg, maps of BMFF) are spatially normalized to a common template using affine and deformable registration, effectively establishing local anatomical correspondence across structures. After spatial normalization, smoothing of the parametric maps is commonly performed to compensate for inaccuracies of the registration step. Spatial normalization and smoothing steps then enable meaningful comparisons between groups of spatially varying data on a voxel-by-voxel or vertex-by-vertex basis. Comparisons are usually performed in the form of general linear models providing the opportunity to incorporate covariates, with the result of these local comparisons being in the form of a statistical map. The identification of specific subregions where the tissue feature under investigation is significantly associated with the variable of interest becomes possible with this approach. The main advantage of SPM is that by removing the anatomical variability in the population study, there is no longer the need of individualized regions of interest for the analyses. Thus, SPM provides the capability of performing analyses that are not biased to one particular region, and it gives an even-handed and comprehensive assessment of feature statistics throughout the different tissues of interest across an entire study population.

Application and Main Findings

Using the SPM framework, Carballido-Gamio et al investigated the local interrelationships of the BMFF measured by MRI and volumetric BMD measured by QCT in the proximal femur of a small group of postmenopausal women.[137] In this pilot study, the authors included 15 postmenopausal women, six without fracture (control group, mean age: 62.4 ± 8 years), and nine with fragility fractures (mean age: 62.8 ± 9 years). Volumetric BMD maps were derived from QCT scans obtained with a calibration phantom, and BMFF maps were derived from CSE-MRI acquisitions at 3T applying six echoes and a multi-frequency model of fat (Figs. 6 and 7).[138] Within-group voxelwise correlations of BMFF and volume BMD were assessed, revealing mostly negative correlations between the BMFF and volumetric BMD across the whole proximal femur.[138] However, the strength of these correlations was spatially heterogeneous, and their spatial distribution was visually distinct between cases and controls (Fig. 7).[138] Thus, SPM-based analysis of CSE-MRI to characterize spatially resolved BMFF may become a promising option for evaluating osteoporotic bone.

Beyond investigating the interrelationships of BMFF and volumetric BMD, CSE-MRI measurements of the

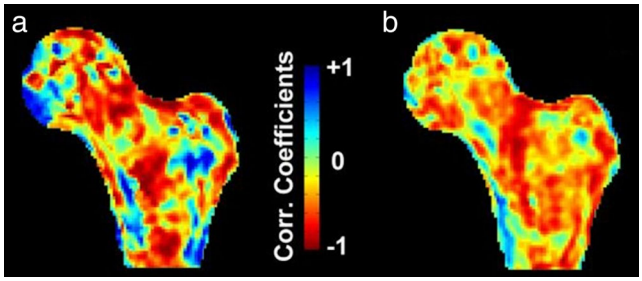

FIGURE 6: Statistical parametric mapping (SPM) of the proximal femur—part I. Maps of Pearson correlation coefficients of the bone marrow fat fraction (BMFF) and volumetric bone mineral density (BMD) for a group of postmenopausal women without fractures (a) and a group of postmenopausal women with fragility fractures (b). Negative correlations between the BMFF and volumetric BMD across the proximal femur were predominantly revealed; however, showing an inhomogeneous spatial pattern of variation.

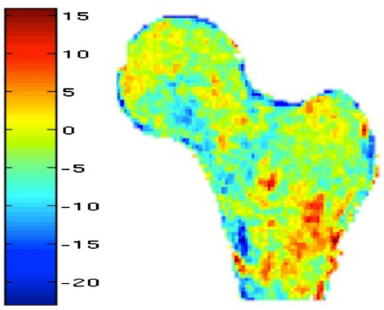

FIGURE 7: Statistical parametric mapping (SPM) of the proximal femur—part II. Color-coded map showing a cross-section of the local differences of bone marrow fat fraction (BMFF) distributions between a group of nine women with fragility fractures and a group of six women without fragility fractures as assessed with water–fat imaging (cases minus controls). A clear pattern of higher BMFF in cases than in controls can be observed in certain regions (eg, the intertrochanteric regions). The scale of the color bar is in percentage of change.

BMFF were recently used to increase the accuracy of QCT measurements of the spine.[139] Furthermore, it was reported that subjects with at least one prevalent vertebral fracture showed decreased MRI stiffness (up to 17.9%) and QCT density (up to 34.2%) at the distal extremities compared to a nonfracture group.[140] High BMFF can lead to false low measurements in single-energy QCT. These errors can be reduced by a factor of five using dual-energy CT or corrections by CSE-MRI measurements of the BMFF and should be considered to investigate the true relationship between BMD and bone marrow adipose tissue in humans.[141] However, it remains to be investigated if such corrections also lead to a better prediction of fracture risk in osteoporotic patients.

Conclusion and Perspectives

Different quantitative MRI methods have been introduced for imaging of osteoporosis at the spine and proximal femur over the last decades, initially based on high-resolution trabecular bone imaging and T_2* mapping. QSM, which can overcome some of the limitations of T_2* mapping, shows also potential for trabecular bone quantifications at the spine, whereas UTE imaging provides surrogate markers of cortical bone quantity and quality. Moreover, MRS and CSE-MRI enable the evaluation of the nonmineralized bone compartment, represented by BM, and extraction of the PDFF. Novel postprocessing and analysis approaches, such as FEA and SPM, have shown potential to further improve the assessment of fracture risk in osteoporotic patients. Thus, MRI is a viable option for radiation-free, quantitative assessment of osteoporotic bone and is fast developing, given the variety of sequences and techniques at hand to date. However, it has to be acknowledged that the methods reviewed in this article have not yet accomplished the ultimate transition to utility in broad clinical routine, which is partially related to limited evidence of clearly improved fracture prediction beyond BMD. Anticipated technical developments and investigations in large representative cohorts, alongside with broader distribution of MRI systems capable of applying these methods, may facilitate quantitative MRI application for osteoporosis imaging in the foreseeable future.

Acknowledgments

None.

REFERENCES

1. NIH Consensus Development Panel on Osteoporosis Prevention Diagnosis and Therapy. Osteoporosis prevention, diagnosis, and therapy. JAMA 2001;285(6):785-795.
2. Compston JE, McClung MR, Leslie WD. Osteoporosis. Lancet 2019; 393(10169):364-376.
3. Consensus Development Conference: Diagnosis, prophylaxis, and treatment of osteoporosis. Am J Med 1993;94(6):646-650.
4. Cooper C, Campion G, Melton LJ 3rd. Hip fractures in the elderly: A world-wide projection. Osteoporos Int 1992;2(6):285-289.
5. Reginster JY, Burlet N. Osteoporosis: A still increasing prevalence. Bone 2006;38(2 Suppl 1):S4-S9.
6. Melton LJ 3rd, Chrischilles EA, Cooper C, Lane AW, Riggs BL. Perspective. How many women have osteoporosis? J Bone Miner Res 1992;7(9):1005-1010.
7. Randell A, Sambrook PN, Nguyen TV, et al. Direct clinical and welfare costs of osteoporotic fractures in elderly men and women. Osteoporos Int 1995;5(6):427-432.
8. Hallberg I, Bachrach-Lindstrom M, Hammerby S, Toss G, Ek AC. Health-related quality of life after vertebral or hip fracture: A seven-year follow-up study. BMC Musculoskelet Disord 2009;10:135.
9. Tarride JE, Burke N, Leslie WD, et al. Loss of health related quality of life following low-trauma fractures in the elderly. BMC Geriatr 2016; 16:84.
10. Bliuc D, Nguyen ND, Milch VE, Nguyen TV, Eisman JA, Center JR. Mortality risk associated with low-trauma osteoporotic fracture and subsequent fracture in men and women. JAMA 2009;301(5):513-521.
11. Bliuc D, Nguyen ND, Nguyen TV, Eisman JA, Center JR. Compound risk of high mortality following osteoporotic fracture and refracture in elderly women and men. J Bone Miner Res 2013;28(11):2317-2324.

12. Center JR, Nguyen TV, Schneider D, Sambrook PN, Eisman JA. Mortality after all major types of osteoporotic fracture in men and women: An observational study. Lancet 1999;353(9156):878-882.
13. Kanis JA, Johnell O, De Laet C, et al. A meta-analysis of previous fracture and subsequent fracture risk. Bone 2004;35(2):375-382.
14. Melton LJ 3rd, Atkinson EJ, Cooper C, O'Fallon WM, Riggs BL. Vertebral fractures predict subsequent fractures. Osteoporos Int 1999;10(3): 214-221.
15. Melton LJ 3rd, Kallmes DF. Epidemiology of vertebral fractures: Implications for vertebral augmentation. Acad Radiol 2006;13(5):538-545.
16. Nevitt MC, Ettinger B, Black DM, et al. The association of radiographically detected vertebral fractures with back pain and function: A prospective study. Ann Intern Med 1998;128(10):793-800.
17. Abrahamsen B, van Staa T, Ariely R, Olson M, Cooper C. Excess mortality following hip fracture: A systematic epidemiological review. Osteoporos Int 2009;20(10):1633-1650.
18. Haentjens P, Magaziner J, Colon-Emeric CS, et al. Meta-analysis: Excess mortality after hip fracture among older women and men. Ann Intern Med 2010;152(6):380-390.
19. Kanis JA, Oden A, Johnell O, De Laet C, Jonsson B, Oglesby AK. The components of excess mortality after hip fracture. Bone 2003;32(5): 468-473.
20. Dyer SM, Crotty M, Fairhall N, et al. A critical review of the long-term disability outcomes following hip fracture. BMC Geriatr 2016;16:158.
21. Magaziner J, Hawkes W, Hebel JR, et al. Recovery from hip fracture in eight areas of function. J Gerontol A Biol Sci Med Sci 2000;55(9): M498-M507.
22. McClung M, Harris ST, Miller PD, et al. Bisphosphonate therapy for osteoporosis: Benefits, risks, and drug holiday. Am J Med 2013;126 (1):13-20.
23. Khosla S, Bilezikian JP, Dempster DW, et al. Benefits and risks of bisphosphonate therapy for osteoporosis. J Clin Endocrinol Metab 2012; 97(7):2272-2282.
24. Cummings SR, Cosman F, Lewiecki EM, et al. Goal-directed treatment for osteoporosis: A progress report from the ASBMR-NOF Working Group on goal-directed treatment for osteoporosis. J Bone Miner Res 2017;32(1):3-10.
25. Lehman RA Jr, Kang DG, Wagner SC. Management of osteoporosis in spine surgery. J Am Acad Orthop Surg 2015;23(4):253-263.
26. Yaacobi E, Sanchez D, Maniar H, Horwitz DS. Surgical treatment of osteoporotic fractures: An update on the principles of management. Injury 2017;48(Suppl 7):S34-S40.
27. Alpantaki K, Dohm M, Korovessis P, Hadjipavlou AG. Surgical options for osteoporotic vertebral compression fractures complicated with spinal deformity and neurologic deficit. Injury 2018;49(2):261-271.
28. Kanis JA. Diagnosis of osteoporosis and assessment of fracture risk. Lancet 2002;359(9321):1929-1936.
29. Kanis JA. Diagnosis of osteoporosis. Osteoporos Int 1997;7(Suppl 3): S108-S116.
30. Ammann P, Rizzoli R. Bone strength and its determinants. Osteoporos Int 2003;14(Suppl 3):S13-S18.
31. Schuit SC, van der Klift M, Weel AE, et al. Fracture incidence and association with bone mineral density in elderly men and women: The Rotterdam study. Bone 2004;34(1):195-202.
32. Engelke K. Quantitative computed tomography-current status and new developments. J Clin Densitom 2017;20(3):309-321.
33. Loffler MT, Sollmann N, Mei K, et al. X-ray-based quantitative osteoporosis imaging at the spine. Osteoporos Int 2019;31:233–250.
34. Link TM. Osteoporosis imaging: State of the art and advanced imaging. Radiology 2012;263(1):3-17.
35. Wehrli FW, Ford JC, Attie M, Kressel HY, Kaplan FS. Trabecular structure: Preliminary application of MR interferometry. Radiology 1991; 179(3):615-621.
36. Wehrli FW, Song HK, Saha PK, Wright AC. Quantitative MRI for the assessment of bone structure and function. NMR Biomed 2006;19(7): 731-764.
37. Majumdar S, Thomasson D, Shimakawa A, Genant HK. Quantitation of the susceptibility difference between trabecular bone and bone marrow: Experimental studies. Magn Reson Med 1991;22(1):111-127.
38. Fazeli PK, Horowitz MC, MacDougald OA, et al. Marrow fat and bone — New perspectives. J Clin Endocrinol Metab 2013;98(3):935-945.
39. Griffith JF, Yeung DK, Antonio GE, et al. Vertebral bone mineral density, marrow perfusion, and fat content in healthy men and men with osteoporosis: Dynamic contrast-enhanced MR imaging and MR spectroscopy. Radiology 2005;236(3):945-951.
40. Reichert IL, Robson MD, Gatehouse PD, et al. Magnetic resonance imaging of cortical bone with ultrashort TE pulse sequences. Magn Reson Imaging 2005;23(5):611-618.
41. Wang Y, Liu T. Quantitative susceptibility mapping (QSM): Decoding MRI data for a tissue magnetic biomarker. Mag Reson Med 2015;73 (1):82-101.
42. Dimov AV, Liu Z, Spincemaille P, Prince MR, Du J, Wang Y. Bone quantitative susceptibility mapping using a chemical species-specific R2* signal model with ultrashort and conventional echo data. Magn Reson Med 2018;79(1):121-128.
43. Krug R, Burghardt AJ, Majumdar S, Link TM. High-resolution imaging techniques for the assessment of osteoporosis. Radiol Clin North Am 2010;48(3):601-621.
44. Krug R, Banerjee S, Han ET, Newitt DC, Link TM, Majumdar S. Feasibility of in vivo structural analysis of high-resolution magnetic resonance images of the proximal femur. Osteoporos Int 2005;16(11): 1307-1314.
45. Kazakia GJ, Carballido-Gamio J, Lai A, et al. Trabecular bone microstructure is impaired in the proximal femur of human immunodeficiency virus-infected men with normal bone mineral density. Quant Imaging Med Surg 2018;8(1):5-13.
46. Chang G, Deniz CM, Honig S, et al. Feasibility of three-dimensional MRI of proximal femur microarchitecture at 3 Tesla using 26 receive elements without and with parallel imaging. J Magn Reson Imaging 2014;40(1):229-238.
47. Chang G, Honig S, Brown R, et al. Finite element analysis applied to 3-T MR imaging of proximal femur microarchitecture: Lower bone strength in patients with fragility fractures compared with control subjects. Radiology 2014;272(2):464-474.
48. Chang G, Rajapakse CS, Regatte RR, et al. 3 Tesla MRI detects deterioration in proximal femur microarchitecture and strength in long-term glucocorticoid users compared with controls. J Magn Reson Imaging 2015;42(6):1489-1496.
49. Banerjee S, Han ET, Krug R, Newitt DC, Majumdar S. Application of refocused steady-state free-precession methods at 1.5 and 3 T to in vivo high-resolution MRI of trabecular bone: Simulations and experiments. J Magn Reson Imaging 2005;21(6):818-825.
50. Han M, Chiba K, Banerjee S, Carballido-Gamio J, Krug R. Variable flip angle three-dimensional fast spin-echo sequence combined with outer volume suppression for imaging trabecular bone structure of the proximal femur. J Magn Reson Imaging 2015;41(5):1300-1310.
51. Wald LL, Carvajal L, Moyher SE, et al. Phased array detectors and an automated intensity-correction algorithm for high-resolution MR imaging of the human brain. Magn Reson Med 1995;34(3):433-439.
52. Sled JG, Zijdenbos AP, Evans AC. A nonparametric method for automatic correction of intensity nonuniformity in MRI data. IEEE Trans Med Imaging 1998;17(1):87-97.
53. Vasilic B, Wehrli FW. A novel local thresholding algorithm for trabecular bone volume fraction mapping in the limited spatial resolution regime of in vivo MRI. IEEE Trans Med Imaging 2005;24(12):1574-1585.
54. Majumdar S, Genant HK, Grampp S, et al. Correlation of trabecular bone structure with age, bone mineral density, and osteoporotic

status: in vivo studies in the distal radius using high resolution magnetic resonance imaging. J Bone Miner Res 1997;12(1):111-118.

55. Bauer JS, Monetti R, Krug R, et al. Advances of 3T MR imaging in visualizing trabecular bone structure of the calcaneus are partially SNR-independent: Analysis using simulated noise in relation to micro-CT, 1.5T MRI, and biomechanical strength. J Magn Reson Imaging 2009;29(1):132-140.

56. Carballido-Gamio J, Phan C, Link TM, Majumdar S. Characterization of trabecular bone structure from high-resolution magnetic resonance images using fuzzy logic. Magn Reson Imaging 2006;24(8):1023-1029.

57. Folkesson J, Carballido-Gamio J, Eckstein F, Link TM, Majumdar S. Local bone enhancement fuzzy clustering for segmentation of MR trabecular bone images. Med Phys 2010;37(1):295-302.

58. Wehrli FW, Gomberg BR, Saha PK, Song HK, Hwang SN, Snyder PJ. Digital topological analysis of in vivo magnetic resonance microimages of trabecular bone reveals structural implications of osteoporosis. J Bone Miner Res 2001;16(8):1520-1531.

59. Gomberg BR, Saha PK, Song HK, Hwang SN, Wehrli FW. Topological analysis of trabecular bone MR images. IEEE Trans Med Imaging 2000;19(3):166-174.

60. Carballido-Gamio J, Krug R, Huber MB, et al. Geodesic topological analysis of trabecular bone microarchitecture from high-spatial resolution magnetic resonance images. Magn Reson Med 2009;61(2): 448-456.

61. Vasilic B, Rajapakse CS, Wehrli FW. Classification of trabeculae into three-dimensional rodlike and platelike structures via local inertial anisotropy. Med Phys 2009;36(7):3280-3291.

62. Saha PK, Xu Y, Duan H, Heiner A, Liang G. Volumetric topological analysis: A novel approach for trabecular bone classification on the continuum between plates and rods. IEEE Trans Med Imaging 2010; 29(11):1821-1838.

63. Chen C, Jin D, Liu Y, et al. Trabecular bone characterization on the continuum of plates and rods using in vivo MR imaging and volumetric topological analysis. Phys Med Biol 2016;61(18):N478-N496.

64. Hotca A, Rajapakse CS, Cheng C, et al. In vivo measurement reproducibility of femoral neck microarchitectural parameters derived from 3T MR images. J Magn Reson Imaging 2015;42(5):1339-1345.

65. Rajapakse CS, Chang G. Micro-finite element analysis of the proximal femur on the basis of high-resolution magnetic resonance images. Curr Osteoporos Rep 2018;16(6):657-664.

66. Knowles NK, Reeves JM, Ferreira LM. Quantitative computed tomography (QCT) derived bone mineral density (BMD) in finite element studies: A review of the literature. J Exp Orthop 2016;3(1):36.

67. Pahr DH, Zysset PK. Finite element-based mechanical assessment of bone quality on the basis of in vivo images. Curr Osteoporos Rep 2016;14(6):374-385.

68. Rajapakse CS, Farid AR, Kargilis DC, et al. MRI-based assessment of proximal femur strength compared to mechanical testing. Bone 2020; 133:115227.

69. Rajapakse CS, Hotca A, Newman BT, et al. Patient-specific hip fracture strength assessment with microstructural MR imaging-based finite element modeling. Radiology 2017;283(3):854-861.

70. Chang G, Hotca-Cho A, Rusinek H, et al. Measurement reproducibility of magnetic resonance imaging-based finite element analysis of proximal femur microarchitecture for in vivo assessment of bone strength. MAGMA 2015;28(4):407-412.

71. Chang G, Rajapakse CS, Chen C, et al. 3-T MR imaging of proximal femur microarchitecture in subjects with and without fragility fracture and nonosteoporotic proximal femur bone mineral density. Radiology 2018;287(2):608-619.

72. Reichenbach JR, Schweser F, Serres B, Deistung A. Quantitative susceptibility mapping: Concepts and applications. Clin Neuroradiol 2015;25(Suppl 2):225-230.

73. Jerban S, Lu X, Jang H, et al. Significant correlations between human cortical bone mineral density and quantitative susceptibility mapping (QSM) obtained with 3D cones ultrashort echo time magnetic resonance imaging (UTE-MRI). Magn Reson Imaging 2019;62:104-110.

74. Chen Y, Guo Y, Zhang X, Mei Y, Feng Y, Zhang X. Bone susceptibility mapping with MRI is an alternative and reliable biomarker of osteoporosis in postmenopausal women. Eur Radiol 2018;28(12):5027-5034.

75. Guo Y, Chen Y, Zhang X, et al. Magnetic susceptibility and fat content in the lumbar spine of postmenopausal women with varying bone mineral density. J Magn Reson Imaging 2018;49(4):1020–1028.

76. Schmeel FC, Luetkens JA, Feisst A, et al. Quantitative evaluation of T2* relaxation times for the differentiation of acute benign and malignant vertebral body fractures. Eur J Radiol 2018;108:59-65.

77. Zhang X, Guo Y, Chen Y, et al. Reproducibility of quantitative susceptibility mapping in lumbar vertebra. Quant Imaging Med Surg 2019;9 (4):691-699.

78. Diefenbach MN, Meineke J, Ruschke S, Baum T, Gersing A, Karampinos DC. On the sensitivity of quantitative susceptibility mapping for measuring trabecular bone density. Magn Reson Med 2019; 81(3):1739-1754.

79. Majumdar S, Genant HK. In vivo relationship between marrow T2* and trabecular bone density determined with a chemical shift—Selective asymmetric spin-echo sequence. J Magn Reson Imaging 1992;2 (2):209-219.

80. Hopkins JA, Wehrli FW. Magnetic susceptibility measurement of insoluble solids by NMR: Magnetic susceptibility of bone. Magn Reson Med 1997;37(4):494-500.

81. Kuhn JP, Hernando D, Meffert PJ, et al. Proton-density fat fraction and simultaneous R2* estimation as an MRI tool for assessment of osteoporosis. Eur Radiol 2013;23(12):3432-3439.

82. Tyler DJ, Robson MD, Henkelman RM, Young IR, Bydder GM. Magnetic resonance imaging with ultrashort TE (UTE) PULSE sequences: Technical considerations. J Magn Reson Imaging 2007;25(2):279-289.

83. Du J, Carl M, Bydder M, Takahashi A, Chung CB, Bydder GM. Qualitative and quantitative ultrashort echo time (UTE) imaging of cortical bone. J Magn Reson 2010;207(2):304-311.

84. Robson MD, Gatehouse PD, Bydder M, Bydder GM. Magnetic resonance: An introduction to ultrashort TE (UTE) imaging. J Comput Assist Tomogr 2003;27(6):825-846.

85. Wan L, Zhao W, Ma Y, et al. Fast quantitative 3D ultrashort echo time MRI of cortical bone using extended cones sampling. Magn Reson Med 2019;82(1):225-236.

86. Araujo Ericky CA, Azzabou N, Vignaud A, Guillot G, Carlier PG. Quantitative ultrashort TE imaging of the short-T2 components in skeletal muscle using an extended echo-subtraction method. Magn Reson Med 2017;78(3):997-1008.

87. Du J, Bydder M, Takahashi AM, Carl M, Chung CB, Bydder GM. Short T2 contrast with three-dimensional ultrashort echo time imaging. Magn Reson Imaging 2011;29(4):470-482.

88. Rahmer J, Bornert P, Groen J, Bos C. Three-dimensional radial ultrashort echo-time imaging with T2 adapted sampling. Magn Reson Med 2006;55(5):1075-1082.

89. Larson PE, Gurney PT, Nayak K, Gold GE, Pauly JM, Nishimura DG. Designing long-T2 suppression pulses for ultrashort echo time imaging. Magn Reson Med 2006;56(1):94-103.

90. Wurnig MC, Calcagni M, Kenkel D, et al. Characterization of trabecular bone density with ultrashort echo-time MRI at 1.5, 3.0 and 7.0 T—Comparison with micro-computed tomography. NMR Biomed 2014; 27(10):1159-1166.

91. Carl M, Bydder GM, Du J. UTE imaging with simultaneous water and fat signal suppression using a time-efficient multispoke inversion recovery pulse sequence. Magn Reson Med 2016;76(2):577-582.

92. Wiesinger F, Sacolick LI, Menini A, et al. Zero TE MR bone imaging in the head. Magn Reson Med 2016;75(1):107-114.

93. Ma YJ, Chen Y, Li L, et al. Trabecular bone imaging using a 3D adiabatic inversion recovery prepared ultrashort TE cones sequence at 3T. Magn Reson Med 2019;83(5):1640–1651.

94. Weiger M, Wu M, Wurnig MC, et al. ZTE imaging with long-T2 suppression. NMR Biomed 2015;28(2):247-254.

95. Manhard MK, Harkins KD, Gochberg DF, Nyman JS, Does MD. 30-second bound and pore water concentration mapping of cortical bone using 2D UTE with optimized half-pulses. Magn Reson Med 2017;77(3):945-950.

96. Rajapakse CS, Bashoor-Zadeh M, Li C, Sun W, Wright AC, Wehrli FW. Volumetric cortical bone porosity assessment with MR imaging: Validation and clinical feasibility. Radiology 2015;276(2):526-535.

97. Reeder SB, Hu HH, Sirlin CB. Proton density fat-fraction: A standardized MR-based biomarker of tissue fat concentration. J Magn Reson Imaging 2012;36(5):1011-1014.

98. Dieckmeyer M, Ruschke S, Cordes C, et al. The need for T(2) correction on MRS-based vertebral bone marrow fat quantification: Implications for bone marrow fat fraction age dependence. NMR Biomed 2015;28(4):432-439.

99. Kugel H, Jung C, Schulte O, Heindel W. Age- and sex-specific differences in the 1H-spectrum of vertebral bone marrow. J Magn Reson Imaging 2001;13(2):263-268.

100. Yeung DK, Griffith JF, Antonio GE, Lee FK, Woo J, Leung PC. Osteoporosis is associated with increased marrow fat content and decreased marrow fat unsaturation: A proton MR spectroscopy study. J Magn Reson Imaging 2005;22(2):279-285.

101. Griffith JF, Yeung DK, Antonio GE, et al. Vertebral marrow fat content and diffusion and perfusion indexes in women with varying bone density: MR evaluation. Radiology 2006;241(3):831-838.

102. Li X, Kuo D, Schafer AL, et al. Quantification of vertebral bone marrow fat content using 3 Tesla MR spectroscopy: Reproducibility, vertebral variation, and applications in osteoporosis. J Magn Reson Imaging 2011;33(4):974-979.

103. Baum T, Yap SP, Karampinos DC, et al. Does vertebral bone marrow fat content correlate with abdominal adipose tissue, lumbar spine bone mineral density, and blood biomarkers in women with type 2 diabetes mellitus? J Magn Reson Imaging 2012;35(1):117-124.

104. Patsch JM, Li X, Baum T, et al. Bone marrow fat composition as a novel imaging biomarker in postmenopausal women with prevalent fragility fractures. J Bone Miner Res 2013;28(8):1721-1728.

105. Schwartz AV, Sigurdsson S, Hue TF, et al. Vertebral bone marrow fat associated with lower trabecular BMD and prevalent vertebral fracture in older adults. J Clin Endocrinol Metab 2013;98(6):2294-2300.

106. Cohen A, Shen W, Dempster DW, et al. Marrow adiposity assessed on transiliac crest biopsy samples correlates with noninvasive measurement of marrow adiposity by proton magnetic resonance spectroscopy ((1)H-MRS) at the spine but not the femur. Osteoporos Int 2015;26(10):2471-2478.

107. Karampinos DC, Ruschke S, Gordijenko O, et al. Association of MRS-based vertebral bone marrow fat fraction with bone strength in a human in vitro model. J Osteoporos 2015;2015:152349.

108. Sheu Y, Amati F, Schwartz AV, et al. Vertebral bone marrow fat, bone mineral density and diabetes: The osteoporotic fractures in men (MrOS) study. Bone 2017;97:299-305.

109. Mistry SD, Woods GN, Sigurdsson S, et al. Sex hormones are negatively associated with vertebral bone marrow fat. Bone 2018;108: 20-24.

110. He J, Fang H, Li X. Vertebral bone marrow fat content in normal adults with varying bone densities at 3T magnetic resonance imaging. Acta Radiol 2019;60(4):509-515.

111. Griffith JF, Yeung DK, Tsang PH, et al. Compromised bone marrow perfusion in osteoporosis. J Bone Miner Res 2008;23(7):1068-1075.

112. Manenti G, Capuani S, Fusco A, Fanucci E, Tarantino U, Simonetti G. Osteoporosis detection by 3T diffusion tensor imaging and MRI spectroscopy in women older than 60 years. Aging Clin Exp Res 2013;25 (Suppl 1):S31-S34.

113. Manenti G, Capuani S, Fanucci E, et al. Diffusion tensor imaging and magnetic resonance spectroscopy assessment of cancellous bone quality in femoral neck of healthy, osteopenic and osteoporotic subjects at 3T: Preliminary experience. Bone 2013;55(1):7-15.

114. Di Pietro G, Capuani S, Manenti G, et al. Bone marrow lipid profiles from peripheral skeleton as potential biomarkers for osteoporosis: A 1H-MR spectroscopy study. Acad Radiol 2016;23(3):273-283.

115. Karampinos DC, Ruschke S, Dieckmeyer M, et al. Quantitative MRI and spectroscopy of bone marrow. J Magn Reson Imaging 2018;47 (2):332-353.

116. Bydder M, Yokoo T, Hamilton G, et al. Relaxation effects in the quantification of fat using gradient echo imaging. Magn Reson Imaging 2008;26(3):347-359.

117. Yu H, Shimakawa A, McKenzie CA, Brodsky E, Brittain JH, Reeder SB. Multiecho water-fat separation and simultaneous R2* estimation with multifrequency fat spectrum modeling. Magn Reson Med 2008;60(5): 1122-1134.

118. Wang X, Hernando D, Reeder SB. Sensitivity of chemical shift-encoded fat quantification to calibration of fat MR spectrum. Magn Reson Med 2016;75(2):845-851.

119. Hernando D, Liang ZP, Kellman P. Chemical shift-based water/fat separation: A comparison of signal models. Magn Reson Med 2010;64(3): 811-822.

120. Colgan TJ, Hernando D, Sharma SD, Reeder SB. The effects of concomitant gradients on chemical shift encoded MRI. Magn Reson Med 2017;78(2):730-738.

121. Liu CY, McKenzie CA, Yu H, Brittain JH, Reeder SB. Fat quantification with IDEAL gradient echo imaging: Correction of bias from T(1) and noise. Magn Reson Med 2007;58(2):354-364.

122. Ruschke S, Eggers H, Kooijman H, et al. Correction of phase errors in quantitative water-fat imaging using a monopolar time-interleaved multiecho gradient echo sequence. Magn Reson Med 2017;78(3): 984-996.

123. Karampinos DC, Ruschke S, Dieckmeyer M, et al. Modeling of T2* decay in vertebral bone marrow fat quantification. NMR Biomed 2015;28(11):1535-1542.

124. Baum T, Yap SP, Dieckmeyer M, et al. Assessment of whole spine vertebral bone marrow fat using chemical shift-encoding based water-fat MRI. J Magn Reson Imag 2015;42(4):1018-1023.

125. Baum T, Rohrmeier A, Syvari J, et al. Anatomical variation of age-related changes in vertebral bone marrow composition using chemical shift encoding-based water-fat magnetic resonance imaging. Front Endocrinol (Lausanne) 2018;9:141.

126. Schmeel FC, Luetkens JA, Enkirch SJ, et al. Proton density fat fraction (PDFF) MR imaging for differentiation of acute benign and neoplastic compression fractures of the spine. Eur Radiol 2018;28(12):5001-5009.

127. Schmeel FC, Luetkens JA, Wagenhauser PJ, et al. Proton density fat fraction (PDFF) MRI for differentiation of benign and malignant vertebral lesions. Eur Radiol 2018;28(6):2397-2405.

128. Sollmann N, Dieckmeyer M, Schlaeger S, et al. Associations between lumbar vertebral bone marrow and paraspinal muscle fat compositions-an investigation by chemical shift encoding-based water-fat MRI. Front Endocrinol (Lausanne) 2018;9:563.

129. Burian E, Subburaj K, Mookiah MRK, et al. Texture analysis of vertebral bone marrow using chemical shift encoding-based water-fat MRI: A feasibility study. Osteoporos Int 2019;30(6):1265-1274.

130. Zhao Y, Huang M, Ding J, et al. Prediction of abnormal bone density and osteoporosis from lumbar spine MR using modified Dixon quant in 257 subjects with quantitative computed tomography as reference. Journal of Magnetic Resonance Imaging; JMRI 2019;49(2):390-399.

131. Shen W, Gong X, Weiss J, Jin Y. Comparison among T1-weighted magnetic resonance imaging, modified dixon method, and magnetic resonance spectroscopy in measuring bone marrow fat. J Obes 2013; 2013:298675.

132. Li G, Xu Z, Gu H, et al. Comparison of chemical shift-encoded water-fat MRI and MR spectroscopy in quantification of marrow fat in postmenopausal females. J Magn Reson Imaging 2017;45(1):66-73.

133. Ruschke S, Pokorney A, Baum T, et al. Measurement of vertebral bone marrow proton density fat fraction in children using quantitative water-fat MRI. MAGMA 2017;30(5):449-460.

134. Martel D, Leporq B, Saxena A, et al. 3T chemical shift-encoded MRI: Detection of altered proximal femur marrow adipose tissue composition in glucocorticoid users and validation with magnetic resonance spectroscopy. J Magn Reson Imag 2019;50(2):490-496.

135. Martel D, Leporq B, Bruno M, Regatte RR, Honig S, Chang G. Chemical shift-encoded MRI for assessment of bone marrow adipose tissue fat composition: Pilot study in premenopausal versus postmenopausal women. Magn Reson Imaging 2018;53:148-155.

136. Friston KJ, Frith CD, Liddle PF, Dolan RJ, Lammertsma AA, Frackowiak RS. The relationship between global and local changes in PET scans. J Cereb Blood Flow Metab 1990;10(4):458-466.

137. Carballido-Gamio J, Karampinos DC, Lai A, Lee S, Krug R. *Investigation of the local relationship between bone marrow fat content and bone mineral density in the proximal femur of subjects with and without fragility fractures*. Baltimore, MD: American Society for Bone and Mineral Research; 2013.

138. Carballido-Gamio J, Harnish R, Saeed I, et al. Proximal femoral density distribution and structure in relation to age and hip fracture risk in women. J Bone Miner Res 2013;28(3):537-546.

139. Cheng X, Blake GM, Guo Z, et al. Correction of QCT vBMD using MRI measurements of marrow adipose tissue. Bone 2019;120: 504-511.

140. Rajapakse CS, Phillips EA, Sun W, et al. Vertebral deformities and fractures are associated with MRI and pQCT measures obtained at the distal tibia and radius of postmenopausal women. Osteoporos Int 2014;25(3):973-982.

141. Cheng X, Li K, Zhang Y, et al. The accurate relationship between spine bone density and bone marrow in humans. Bone 2020; 115312:134.